AgriCarbon-EO v1.0.1: Large Scale and ~~High Resolution~~ High-Resolution Simulation of Carbon Fluxes by Assimilation of Sentinel-2 and Landsat-8 Reflectances using a Bayesian approach

Taeken Wijmer[1,2,*], Ahmad Al Bitar[1,*], Ludovic Arnaud[1], Remy Fieuzal[1], and Eric Ceschia[1]

[1]CESBIO, Université de Toulouse, CNES/CNRS/INRAE/IRD/UPS, 18 Avenue Edouard Belin, bpi 2801, CEDEX 09, 31401 Toulouse, France

[2]DYNAFOR, Université de Toulouse, INRAE, INPT, INP-PURPAN, Castanet-Tolosan, France

Correspondence: Taeken Wijmer (taeken.wijmer@cesbio.cnes) and Ahmad Al Bitar (ahmad.albitar@gmx.com)

Abstract. Soil organic carbon storage is a ~~well identified~~ well-identified climate change mitigation solution. ~~The extensive in-situ monitoring~~ An extensive quantification of the soil carbon storage in cropland for agricultural policy and offset carbon markets ~~is prohibitive~~using in-situ measurements would be excessively costly, especially at ~~intra-field~~ the intrafield scale. For this reason, comprehensive ~~Monitoring, Reporting and Verification~~ monitoring, reporting, and verification (MRV) of soil carbon and its explanatory variables at ~~large scale needs~~ a large scale need to rely on remote sensing and modelling tools that provide the ~~spatio-temporal~~ spatiotemporal dynamics of the carbon budget ~~and it's components at high resolution with associated uncertainties~~components with the associated uncertainties at high resolution. In this paper, we present AgriCarbon-EO v1.0.1: an end-to-end processing chain that enables the estimation of carbon budget components of major crops and cover crops at ~~intra-field~~ intrafield resolution (10 m) and large scale (over 110x110 km) by assimilating remote sensing data in physically-based radiative ~~transfert~~ transfer and agronomic models. The data assimilation in AgriCarbon-EO is based on a novel Bayesian approach that combines ~~Normalised Importance Sampling~~ normalized importance sampling (NIS) and ~~Look-Up Table~~ look-up table (LUT) generation. This approach propagates the uncertainties across the processing chain from the reflectances to the output variables. The chain ~~considers as input a~~ inputs are land cover maps, ~~multi-spectral~~ multispectral reflectance maps from the Sentinel-2 and Landsat-8 satellites, and daily weather forcing. ~~The~~ In the first step, inverse modelling of the PROSAIL radiative transfer model ~~is inversed in a first step to obtain Green Leaf Area Index~~ was performed to obtain the green leaf area index (GLAI). The GLAI time series are then assimilated into the SAFYE-CO2 crop model while taking into consideration their ~~uncertainty. The~~ uncertainties. After a presentation, the chain is applied over winter wheat in the ~~south-west~~ southwest of France during the cropping seasons from 2017 ~~and~~ to 2019. We compare the results ~~agaisnt~~ against the net ecosystem exchange measured at the FR-AUR ICOS flux site (RMSE = ~~1.69~~ 1.68 - ~~2.4~~ 2.38 $\mathrm{gC\,m^{-2}}$, $R^2 = \underline{0.88}0.87 - \underline{0.88}0.77), biomass (RMSE = \underline{250}11.34 \mathrm{g\,m^{-2}}, R^2 = \underline{0.9}0.94), and \underline{combine harvester yield maps. We quantify} yield maps obtained from combine harvesters. We als$

$-47 \mathrm{g\,m^{-2}}, -39\% variability), and the impact of the number of remote sensing acquisitions on the outputs (-66\% of mean uncertaint$

Keywords: MRV; Carbon Farming; crop modelling; Sentinel-2; ~~Normalised~~ Normalized Importance Sampling

Copyright statement.

1 Introduction

Agriculture and land use changes ~~accounts~~ account for 15% ~~*ie*~~ *i.e.* (8.7 Gt $\mathrm{CO}-2\ \mathrm{yr}^{-1}$) of ~~human induced Green House Gas~~ human-induced greenhouse gas (GHG) emissions (**??**). ~~On the other hand, agriculture~~ Agriculture has also been identified as a sector ~~where climate mitigation solutions can be implemented~~ that can contribute to climate mitigation through several solutions (**??**). Among ~~those solutions, soil carbon~~ these, soil organic carbon (SOC) storage has the potential to remove 0.6 to 9.3 Gt $\mathrm{CO}-2\ \mathrm{yr}^{-1}$) from the atmosphere through the implementation of carbon farming practices ~~worldwide (**?**). For cropland, soil carbon storage~~ (**?**). Increasing the SOC implies an enhancement of the net ecosystem carbon budget (NECB) (**?**,**?**,**?**)expressed in Equation **??**. A positive variation of NECB can be achieved by increasing the gross primary production (GPP) and the net ecosystem exchange (NEE) through aboveground crop residue retention (**?**,**?**), the addition of cover crops in crop rotations (**??**), ~~reduced tillage (**?**),~~ and an increase of the carbon imports through the application of organic amendments ~~(**?**)~~ (**?**) and biochar (**?**). ~~Moreover, organic carbon storage~~

Equation **??** also shows the importance of 1) the quantification of the effect of ecosystem respiration (Reco) which is subdivided into autotrophic (plant) and heterotrophic (soil) respiration (Rauto and Rh), and 2) the quantification of carbon exports that mainly correspond to yield and the fraction of biomass incorporated to the soil.

It should be noted that after the death of the vegetation, all the unharvested biomass returns to the soil. At this point, we can approximate that NECB = DeltaSOC. The accumulation of SOC in agricultural soils, in addition to climate change mitigation, has additional benefits in terms of ~~Ecosystem Soil Services~~ ecosystem soil services (ESS)~~like~~ , such as increasing soil fertility (**?**), ~~enhanced~~ enhancing water holding capacity (**?**) ~~or higher~~ and increasing biodiversity (**?**). ~~Soil Organic Carbon (SOC)~~ SOC storage could also ~~account for~~ provide an additional source of revenue for farmers through carbon credits and subsidies. ~~To assess the amounts of sequestered carbon as well as the impact on agro-ecosystems an objective and reliable quantification of the carbon budget and crop growth variables is needed.~~

Following the Intergovernmental Panel on Climate Change guidelines for national GHG inventories, methodologies for assessing SOC stock changes ~~and GHG emissions~~ have been developed. They are based on a tiered approach with increasing complexity involving ~~activity and soil data compilation up to~~ soil monitoring networks where SOC is directly measured and process-based modelling where Delta SOC is modelled by taking into account the soil, climate, and mean biomass returned to the soil (GPP-Rauto-Cexport) derived from yield at theregional scale (e.g. Yasso07 in Finland, RothC in Japan, DayCent in the USA)~~tailored to national context~~. The need to monitor soil carbon at ~~Farm level~~ the farm and field levels to inform individual farmers, and guide policies and the development of carbon markets has led to the development of ~~Monitoring Reporting and Verification~~ monitoring reporting and verification (MRV) schemes based on similar ~~aproaches~~ approaches employed at a higher resolution (**??**). ~~Those~~ These approaches are mainly used in carbon farming projects following national or regional initiatives (e.g. Label Bas Carbone in France). They often rely on a ~~soil centered quantification approaches which has limitations in terms of accuracy and reliability of the soil and biomass input data and a field scale resolution that~~ soil-centred quantification approach where the focus is the modelling of Rh, Cimports, and Cexports. In these approaches, the estimates of carbon returned to the soil are usually extrapolated from farm- or field-scale yield information (?). The field-scale often does not match the ~~spatial resolution of in-situ soil~~ intra-field/farm variability of the soil characteristics and plant growth ~~variability (??). Tools including coupled~~ (??). This means that these values present limitations in terms of accuracy and spatial representativity.

Coupled plant/soil process-based models ~~are used to address the spatial representativity challenge and quality of biomass data monitoring~~that address the quality and quantity of the crop residues that return to the soil are also used to assess SOC stock changes. These models include the main components of the cropland's ~~carbon budget, plants photosynthesis, and respiration, emission due to soil organic matter mineralisation. These models~~ biological $CO-2$ fluxes. They can also account for carbon ~~imports through organic fertilisation~~ inputs through organic fertilization and carbon exports of biomass at harvest ~~(?). State of the art agronomic models e.g.~~ (Equation **??**, (?). Existing agronomic models such as, DSSAT-CSM (?), ~~soil models~~ STICS (Launay et al., 2021), DAYCENT (Parton et al., 1998) and WOFOST (?), soil models, e.g. DNDC (?), and land surface models, e.g. ORCHIDEE-STICS ~~, (?)~~(?), take into account a ~~large~~ wide array of environmental conditions to represent crop growth and the components of the carbon budget ~~components (Net Ecosystem Exchange - NEE, Gross Primary Production - GPP, autotrophic respiration - Ra, heterotroph respiration - Rh), of the crop biomass, and of the yield variables~~(Equation **??**). However, water and nutrient availability, local topography, pests, and ~~historic~~ historical factors (e.g. former ditches, roads, field limits) highly influence ~~the~~ soil and plant processes (?). This can ~~results in high spatio-temporal~~ result in high spatiotemporal variability in crop development and soil processes that can be observed even at ~~intra-field~~ the intrafield scale (**??**). Moreover, to operate those models, farmer activity data and crop development dynamics are required ~~in order~~ to provide accurate estimates of SOC stock changes. Getting hold ~~on~~ of this information at a large scale is still ~~very~~ challenging (**??**). ~~Yet~~ However, it is possible to use time series of biophysical variables such as GLAI, derived from remote sensing data, to provide information about development dynamics to those models through data assimilation ~~(???)~~(**???**). These assimilated observations ~~allow to~~ provide spatially explicit ~~crop specific~~ crop-specific estimates of biomass and carbon ~~restituted~~ returned to the soil using coupled soil-plant models. Assimilation ~~exercises~~ of biophysical variables ~~are~~ is usually based on iterative optimization methods such as Simplex, Monte-Carlo Markov Chain ~~, Ensemble~~ (MCMC), ensemble Kalman filter, or variational assimilation that are generally applied at moderate resolutions (**??**) or field ~~scales (??). It is often computationally prohibitive to apply~~ scale (**??**). Applying those methods at ~~intra-field~~ an intrafield resolution over large areas ~~. This issue of scalability is key as solving it is a major stepping stone to assess~~ is often computationally prohibitive. Enhancing scalability is thus key to assessing the spatial variability of ~~the CO-2 flux components .~~ $CO-2$ flux components at a scale consistent with measurements of soil and plant characteristics. Operating on a scale that is representative of measurements enables better diagnosis and calibration of plant and soil processes, as well as a more robust validation and uncertainty estimation of the model outputs.

~~The knowledge of this variability is in it's turn a major asset to define soil sampling strategies, assure spatial coherency of model validation shemes, and modulate precision farming practices.In this paper , we address this challenge by presenting~~

The aim of this paper is to present the newly developed AgriCarbon-EO ~~processing-chain~~ processing chain for the assimilation of ~~EO~~ Earth Observation (EO) data into the SAFYE-CO2 agronomic model ~~(??)~~ at large scale (100 km) and ~~intra-field~~ intrafield resolution (10 m). ~~These spatial resolutions and scales are achieved~~ This processing chain allows for the assessment of the carbon budget components (Equation **??**). The challenge of estimating the carbon budget components at high spatial resolution at a large scale is addressed by using the new BASALT (~~Bayesian Normalised Importance sampling via Look-Up~~ BAyesian normalized importance SAmpling via Look-up Table generation) algorithm~~that~~, which also provides uncertainty estimates. In ~~AgriCarbon-EO, BASALT is used to inverse the PROSAIL (?) radiative transfer model to Obtain GLAI at 10 m resolution, GLAI that is thereafter assimilated into the SAFYE-CO2 crop model. In~~ addition, the paper ~~also aims at: evaluating the accuracy~~aims to provide an evaluation of the accuracy, limitations, and robustness of AgriCarbon-EO ~~outputs through a multi-scale validation and coherency exercise; assessing the benefit of high resolution EO data assimilation through a spatial (pixel vs field)and temporal (single vs multi-mission) analysis; verifying the coherency of the outputs through intra-field as well as regional analysis~~methods through validation exercises and scenario simulations. We chose to make these assessments for wheat in Southwest France, as this area benefits from a large amount of data that has been gathered in the context of the Observatoire Spatial Regional (OSR), and the Integrated Carbon Observation System (ICOS) network. Furthermore, Southwest France is a major production area of wheat. This area has also been chosen because it presents a challenge for spatial crop modelling in reproducing the diverse crop growth dynamics induced by a wide array of pedo-climatic conditions in a hilly landscape. The scenario simulations were designed to assess the robustness of the method with respect to the amount of assimilated remote sensing data, and the added value in using high-resolution agronomic modelling.

In the following sections, we first present the details of the AgriCarbon-EO ~~processing-chain~~ processing chain including the standard inputs, ~~the modelsand the~~ models, and BASALT assimilation scheme. We then present the numerical experimental setup and the validation ~~data-sets~~datasets. Next, we present the validation results ~~, and the spatial analysis results. Finallywe conclude on~~ and the impact of image availability. Finally, we conclude with the benefits and ~~the~~ limitations of the presented solution for assessing the cropland carbon budget components and their associated uncertainties at high resolution over large areas.

2 AgriCarbon-EO chain

2.1 Overview of the processing chain

AgriCarbon-EO is an end-to-end processing chain that simulates multiple relevant variables of crop development, biomass inputs to the soil, ~~and~~ CO-2 fluxes, and water at a daily timescale~~and over large territories~~, for the assessment of carbon and water budgets. It is specifically designed to assimilate optical remote sensing datasets at native high resolution into a simple but generic agronomic model (SAFYE-CO2) over large territories. ~~All the processing steps are conceived in a comprehensive manner (Fig.1). A brief point wise~~ A brief description of the data flow and processing steps is presented here (Figure 1) and detailed in the following subsections:

1. A ~~pre-processing~~ preprocessing "Data ingestion" step allows the updating of existing ~~data sets~~ datasets through automated downloading of satellite images and weather forcing. Optical ~~Bottom Of Atmosphere~~ bottom of atmosphere

(BOA) reflectances are downloaded for Sentinel-2 and Landsat-8 (referred to as S2 and L8 below). Satellite data are uncompressed and relevant spectral bands are stacked. The weather data ~~is~~ are stored in time series with the associated correspondence matrix to the ~~high resolution~~ high-resolution grid defined by the user. This is ~~done~~ performed for the zone defined by the input land cover ~~polygon shapefile~~(polygons or mask raster map).

2. The biophysical variable GLAI is retrieved from the satellite reflectance images by inverting a radiative transfer model (PROSAIL). The retrieval of GLAI is based on an adapted Bayesian importance sampling procedure (*i.e.* BASALT). In this step, a spatial application of the retrieval model is done for each satellite image~~independently~~.

3. The crop model (SAFYE-CO2) parameters are inverted by assimilating the GLAI time series using the ~~same Bayesian importance sampling method (BASALT) as in step two~~BASALT method as in the previous step. In this case, LUTs are generated based on the closest known weather ~~record~~simulation node. Only the phenological crop model parameters and ~~Ligth Use Efficiency~~the light use efficiency (LUE) are inverted in this procedure.

4. A ~~post-processing~~ postprocessing step allows the construction of the output products based on the ~~a posteriori~~ posterior crop model parameter distribution. ~~Geo-referenced~~ Georeferenced maps of the variables of interest in each model (*i.e.* PROSAIL, SAFYE-CO2) are constructed as well as cumulative variables (e.g. NEP ~~that~~ which is the cumulative NEE over one ~~corpping~~ cropping year, number of satellite acquisitions, and soil water content~~, etc.~~).

AgriCarbon-EO is implemented in the Python language. A maximum requirement of 5 GB per process ~~,~~ for the satellite images needs to be considered. ~~These requirements allow mono process~~ This will allow mono-process tests and development on standard computers over smaller study areas, as well as ~~large scale~~ large-scale applications (e.g. 100x100 km) with ~~HPC~~ high-performance computing (HPC) resources.

2.2 Input dataset

In the following subsections, the spatial datasets needed for AgriCarbon-EO are detailed with the corresponding sources~~for the current study~~.

2.2.1 ~~Landcover~~ Land cover map

The main driver for the data preparation is a ~~Land Cover~~ land cover (LC) map in vector ~~shapefile format~~ format (shapefile). This file should contain the boundaries of each agricultural field for a given cropping year over a selected region of interest (*i.e.* border extents of the LC shapefile). Based on the border extents of the LC ~~shapefile~~ map, the remote sensing and weather forcing data are downloaded and ~~pre-processed~~preprocessed. When the simulations are intended to cover several cash crop cycles a ~~multi~~ run scenario of AgriCarbon-EO is considered for each individual crop cycle. Additionally, a standard simulation can include a cover crop with each cash crop~~so that the full cropping year can be taken into account~~. In this paper, AgriCarbon-EO was applied ~~for the~~ to winter wheat crops in ~~south-west of~~ Southwest France (on the Sentinel-2 tile referenced as 31TCJ) ~~over~~ in 2017, 2018, and 2019. The LC ~~shapefile~~ map was obtained from the Registre Parcellaire Graphique (RPG) in France

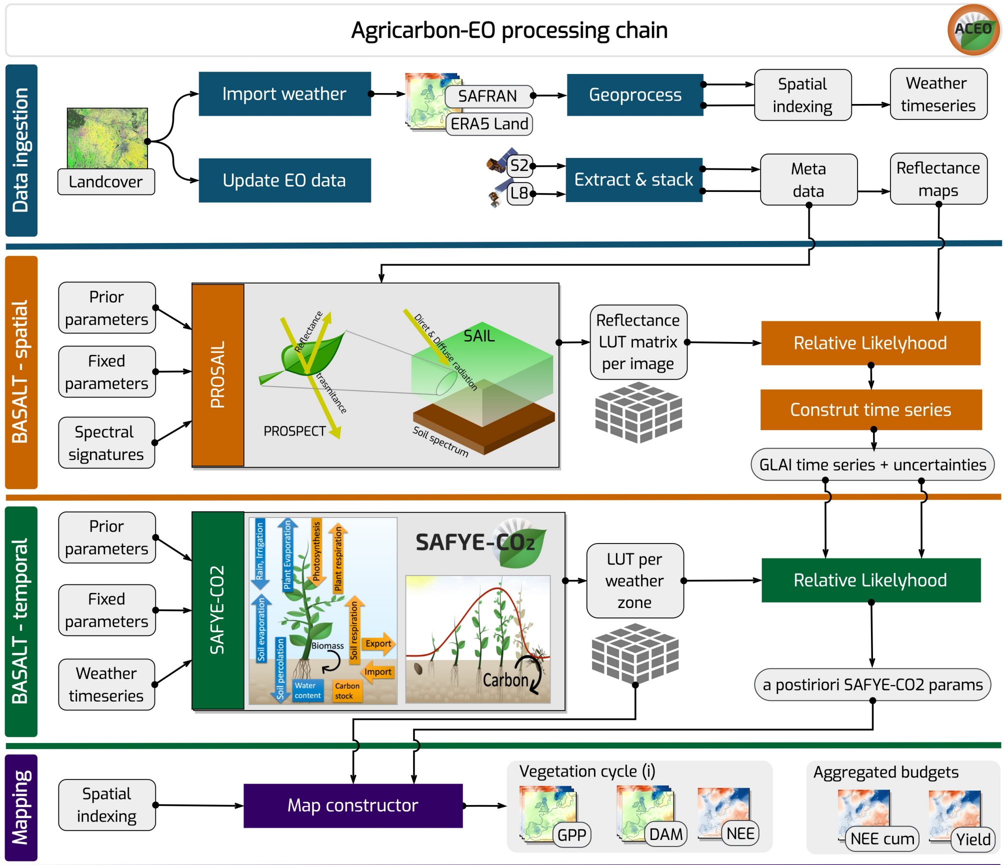

Figure 1. Overview of the AgriCarbon-EO data flow and main processing steps that include the data ingestion, BASALT spatial retrieval, BASALT temporal retrieval, and mapping of the variables of interest.

(“RPG,” 2021), which is available online in open licence v2.0. This information is produced by the Institut Geographique National (IGN) for the Agence de Service de Paiement (ASP *i.e.* The French Paying Agency) in charge of the implementation, control, and payment of the subsidies for the EU Common Agricultural Policy (CAP) in France. ~~The original maps which are in~~ In this study, the original polygons in the Lambert-93 projection (EPSG:2154 - RGF93) ~~are reprojected to the~~ were reprojected to a selected common grid projection~~in AgriCarbon-EO~~, WGS 84/UTM31~~in this case~~.

2.2.2 BOA surface reflectances

The assimilated remote sensing data are optical surface reflectances at ~~Bottom Of Atmosphere (BOA)~~the BOA, which correspond to reflected energy from the top of the canopy and the soil at a given incidence angle, for a set of observed spectral bands. Currently, AgriCarbon-EO ~~is conceived to use data from EU Copernicus program~~ uses data from the ESA’s Sentinel-2 program (**?**) and NASA’s Landsat-8 program (**?**), knowing that the modular interface is compatible with ~~multi-source~~ multisource EO data. The Sentinel-2 data are acquired over 13 optical bands with a resolution of 10 to 60 m depending on the spectral bands with a ~~5 days~~ 5-day revisit from the constellation. Only the nine visible bands ~~are~~ were considered from the Landsat-8 data. Landsat-8 has a revisit of 16 days and a spatial resolution of 30 m in the visible range.

For this study, the data were downloaded from the Thematic ~~centre for continental surfaces~~ Center for Continental Surfaces (THEIA)~~that~~, which uses a common atmospheric correction and cloud masking algorithm for Sentinel-2 and Landsat-8 through the MAJA processing chain (?). This enables a ~~harmonised~~ harmonized Level-2A database with an efficient cloud masking algorithm (?). The data ~~contains quality indicators~~contain quality indicators, including cloud coverage. The datasets are presented as granules (tiles) of 110x110 km ~~ortho-images~~ orthoimages in the UTM projection. Prior to the processing, the remote sensing datasets are decompressed ~~, re-sampled~~ and resampled at 10 m resolution using ~~nearest neighbour~~nearest-neighbour.

2.2.3 Weather forcing data

Daily weather data maps covering the simulation period and spatial extents are used to force the crop model. Cumulative daily global incoming solar radiation ~~, Rg in $\mathrm{W\,m^{-2}}$~~ (Rg in $\mathrm{MJ\,m^{-2}}$) and daily average air temperature at 2 m ~~,~~ (Ta in °C) are needed for the vegetation growth module in SAFYE-CO2. Based on previous studies that showed the impact of diffuse radiation on crop development and photosynthesis (??), the diffuse incoming radiation is computed based on ?. Furthermore, ~~when~~ two additional datasets are needed for the water budget module of SAFYE-CO2~~is activated ,~~: daily potential evapotranspiration ~~,~~ (ET0 in $\mathrm{mm\,d^{-1}}$~~,~~) and daily cumulative rainfall ~~in $\mathrm{mm\,d^{-1}}$ are extracted from the weather data~~(Rain in $\mathrm{mm\,d^{-1}}$). AgriCarbon-EO supports two data sources that provide weather data: the Météo-France SAFRAN dataset (?) and ~~the~~ ERA5 Land (?). The extraction of the ERA5 Land data ~~is done~~ was performed via the dedicated API. SAFRAN consists ~~in~~ of a reanalysis of climate variables at 8 km spatial resolution and the hourly timescale over France starting 1958. In this paper, the ~~water module is deactivated and only the weather data (Rg and Ta) is~~ weather data were extracted from the Météo-France SAFRAN dataset and ~~re-projected~~ reprojected over the UTM/31N at 8 km resolution.

2.3 Process-based models

2.3.1 Radiative transfer modelling using PROSAIL

Maps of geophysical variables (*i.e.* GLAI) are retrieved in AgriCarbon-EO by inverting the PROSAIL radiative transfer model. PROSAIL ~~was~~ has been extensively used as a radiative transfer model for vegetated areas ~~over~~ (?) with a wide range of inversion schemes (?). PROSAIL combines the PROSPECT and ~~the~~ SAIL models (?). PROSPECT provides leaf spectral properties in the 400 nm to 2500 nm ~~band width~~ wavelength (?). SAIL (~~Scattering by Arbitrary Inclined Leaves~~scattering by arbitrary inclined leaves) is a multidirectional canopy reflectance model (?) based on the bidirectional reflectance model (?). ~~PROSAIL and its subsequent versions have been widely used for remote sensing applications (?). The python~~ A Python implementation of PROSAIL ~~is~~ was used in AgriCarbon-EO. This version includes the coupled PROSAIL from PROSPECT-5-D (?), 4SAIL (?), and a ~~Simple~~ simple Lambertian soil reflectance model. ~~PROSAIL parameters are~~ The PROSAIL parameters were inverted using a Bayesian approach in order to provide GLAI and its corresponding uncertainty as input to the crop model inversion.

2.3.2 Crop ~~CO − 2~~ CO2 fluxes and biomass modelling using SAFYE-CO2

SAFYE-CO2 is a parsimonious agronomic model that runs at a daily time-step (**???**). The model stems from the SAFY models (**??**) which ~~computes Dry Above ground bioMass (DAM)~~compute DAM, based on the ~~Light-Use Efficiency (LUE)~~ LUE theory of **?**. ~~In Contrast with SAFY,~~ A full description of the SAFYE-CO2 model ~~computes the Gross Primary Production (GPP) based on an effective LUE (ELUE) (**?**). Where Rg is the incoming global radiation ($\mathrm{MJ\,m^{-2}d^{-1}}$), Ec is the extinction coefficient, FAPAR is the Fraction of Absorbed Active Radiation, f-T(Ta) is the temperature stress function that depends on Ta the mean air temperature at 2 m (°C), f-w(WC) is the water stress function where WC is the soil water content ($\mathrm{m^{-3}m^{-3}}$). In this study, the water stress function is deactivated (*i.e.*f-w(WC) = 1), ELUE ($\mathrm{gC\,MJ^{-1}\,m^{-2}}$) is the effective Light Use Efficiency function. Where~~ is provided in **???**. The core equations of the model are detailed below. where LUE-a ($\mathrm{gC\,MJ^{-1}\,m^{-2}}$) is the light use efficiency for direct radiation and LUE-b is a correction coefficient for the impact of diffuse radiation ~~on LUE~~Rdiff ($\mathrm{MJ\,m^{-2}d^{-1}}$) on ELUE.

In Equation **??**, SR10 ~~is a multiplicative factor that takes into account the decrease of~~ accounts for the decrease in photosynthetic efficiency during senescence ~~.~~

~~The Net Primary Production NPP ($\mathrm{gC\,m^{-2}}$) is computed from the GPP ($\mathrm{gC\,m^{-2}}$) by subtracting the autotrophic respiration Rauto ($\mathrm{gC\,m^{-2}}$). Rauto is divided into vegetation maintenance respiration Rmaint (**?**) and vegetation growth respiration Rgrow (**?**).~~

~~Rmaint is computed using a mainteoef and SR10 to represent an increase in relative maintenance cost during senescence. The maintenance coefficient depends on temperature, and two parameters: the basal respiration at 10°C (R10) and the soil respiration (Q10).~~

~~The growth respiration is computed from the growth conversion efficiency, the GPP and Rmaint.~~

~~The NEE ($\mathrm{gC\,m^{-2}}$) is then computed by substracting the heterotrophic respiration Rh from the NPP. The Rh ($\mathrm{gC\,m^{-2}}$) is computed based on the empirical model in (**?**) that depends on soil moisture and temperature.~~

~~Where Rh-1 is the reference heterotrophic respiration rate, Rh-2 expresses the RH sensitivity to temperature and H-water-stressis the effect of soil moisture on soil carbon decomposition.~~

~~Where RhH1 and RhH2 provide the form of the water stress function and RSM1 The relative soil moisture~~linked among others to the decrease in chlorophyll. where Cs is the parameter that controls the slope of SR10 depending on the thermal age of the crop SMT and Sen-a refers to the thermal age at which the plant enters senescence.

The ~~NPP ($\mathrm{gC\,m^{-2}}$) is divided into root and above ground NPP using a root biomass allocation approach (**?**). The root biomass allocation~~ fraction of biomass allocated bellowground PRTR is ~~defined~~ computed using PRTRa, PRTRb, PRTRc, and SMTG which ~~are respectively the end of cycle biomass allocation to roots~~correspond to the end-of-cycle fraction of biomass allocated below-ground, the initial ~~biomass allocation to roots~~fraction of biomass allocated belowground, a coefficient modulating the decrease in ~~Biomass~~ biomass partition to the roots between the initial and ~~end of cycle state~~end-of-cycle states, and the sum of the temperature at which grain filling starts respectively. The fraction of above-ground biomass allocated to the leaves PRTL is computed using PRTLa and PRTLb0, respectively, the initial fraction of the above-ground biomass that is not allocated to the leaves and a fitting parameter that modulates the rate and thus the end of allocation of above-ground biomass to the leaves.

The biomass and yield are used to determine carbon exports in Equation **??**. Equation **??** illustrates a simple way to estimate exported biomass by taking into account only the dry above-ground biomass (DAM), the harvest index (HI), and the fraction of carbon in the dry biomass (Cveg).

~~The DAM and Dry Below Ground Mass DBM~~ ~~($g\,m^{-2}$)~~ ~~are computed from NPP~~

~~From the change of DAM the green leaf area index change is computed depending on growth or senescence periods, starting from the date of emergence emerg. Where SLA~~ ~~($m^2\,g^{-1}$)~~ ~~is~~ The growth respiration is computed from the ~~specific leaf area and PRTL is the DAM to leaf biomass partitioning. PRTLa and PRTLb are fitting parameters and SMT is the sum of effective temperature (°C)since emergence. Where sen-a~~ growth conversion efficiency, GPP, and Rmaint.

Rh-1 is the ~~sum of temperature (°C)at senescence and sen-b~~ reference Rh rate, Rh-2 expresses the RH sensitivity to temperature, and H-waterstress is the ~~rate of senescence. Eq. (??, ??)provide the link between the modeled GLAI and the GLAI retrieved from optical EO and therefore allows to constrain the model's phenological and light use efficiencyparameters (emerg, PRT~~effect of soil moisture on soil carbon decomposition. In H-water~~La, PRT~~stress, Rh~~Lb, SLA, sena, senb, Harv, LUEa) using EO data assimilation. Note that, the water fluxes computation in SAFYE-CO2 are based on the Penman-Monteith and FAO-56 methodologies that enables to compute the evapotranspiration and~~ H1 and RhH2 provide the form of the water ~~distribution in the~~ stress function and RSM1 the relative soil ~~based on a bucket model (?). The coupling between the carbon and water cycle is two ways. The plant growth impacts the root wateruptake and the soil water content impacts the GPP production through a water stress coefficient. Detailed description of the SAFY-CO2 and SAFYE-CO2 model is provided in (?) and (?). In this paper, the water-carbon coupling is deactivated. The soil stress impact on the vegetation cycle scale is implicitly considered through the assimilation of GLAI. The relative parsimony of SAFYE-CO2 compared to models such as STICS (?) or DSSAT (?) that have a finer description of the plant, climate and soil processes results in a limited number of model inputs. A new python~~ moisture.

A Python implementation of SAFYE-CO2 was developed for AgriCarbon-EO and is used in this paper. This new version is ~~vectorised in order~~ vectorized to provide predictions for ~~multi-runs~~ multiple runs and build LUTs. It can also handle multiple vegetation cycles for each run (e.g. crop and cover crop) ~~,~~ and has a modular architecture. The physical modules are restructured to regroup soil processes, plant phenology, plant physiology, ~~heterotroph activity~~heterotrophic activity, and field management.

2.4 ~~Bayesian normalised importance SAmpling using Look out Table - BASALT~~

~~Answering the need for large-scale high resolution assimilation in AgriCarbon-EO led to the development of a tailored inversion method. The new approach, BASALT, involves the bayesian Normalised Importance Sampling (NIS) approach to answer the need for uncertainty propagation across the processing chain, and Look-Up Tables (LUT) generation that provides computational gain by reducing the total number of model simulations. In a Bayesian framework, the initial knowledge about the model~~In SAFYE-CO2, the water flux computation is based on the Penman-Monteith and FAO-56 methodologies that enable the computation of evapotranspiration and water distribution in the soil based on a bucket model (?). The coupling between the carbon and water cycles occurs in two ways. Plant growth impacts root water uptake, and the soil water content impacts GPP production through a water stress coefficient. The dynamic computation of GLAI in Equation ?? provides the link between the model and the GLAI retrieved from optical EO and therefore allows us to constrain the model's ~~parameters is represented by a probability distribution P(Θ),~~ *~~theso − calledpriordistribution.Theknowledgebroughtbytheobservationsxisexpressedbytheconditio~~*

~~In our case MCMC based approaches are computationally inadequate because they would impose dependent iterative procedures over a v~~ ~~but not to the assimilation of satellite imaging. Actually, when the processed entities are numerous for a similar set of forcing inputs (*i.e.* weather grid), the iterative inversion produces a considerable amount of common solutions in the explored parameter space (*i.e.* samples) . Those common solutions hint at the possibility to use a LUT for each group of entities that share a common forcing and evalua~~ ~~La, PRTLb, SLA, sena, senb, Harv, LUEa) using EO data assimilation. The assimilation of GLAI allows implicit accounting of soil stress~~ ~~new solution changes. When the number of entities to inverse is large (e.N » n) and (t-eval« t-run) , this approach requires less simulations~~ ~~or DSSAT (?) entails a limited number of free parameters controlling the vegetation dynamics. This, allows the use of scalable assimilatio~~

~~.~~

~~3.1 Log-likelyhoods computations~~

~~In practice when evaluating the different LUT entries (i. e weather grid points, images) over a given pixel, we compute log-likelyhoods to~~

~~2.4 Bayesian normalized importance SAmpling using Look out Table - BASALT~~

~~where~~ v is the simulation value, mu and sigma are the mean and standard deviation of the observation, j is the index for entities, ~~o~~ is the index of the independent observations, and i is the index for the model run in the LUT. ~~Naive implementation of this expression leads~~ ~~simple and efficient vanilla matrix product. To represent the likelyhoods using float numbers the log-likelyhoods are re-scaled by their ma~~ ~~w~~ is the weighted mean, v-x ~~is~~ the vector given by the LUT for a parameter or variable, ~~and x x is~~ the number of samples ~~. Where and~~ sigma-w is the weighted standard deviation.

~~In summary the processing steps for BASALT are the following:~~

~~4.1~~ Retrieval of GLAI maps from PROSAIL

When inverting PROSAIL, the main objective is to retrieve ~~the GLAI and GLAI and its~~ associated uncertainties that will be assimilated by SAFYE-CO2. This is done by generating ~~a an~~ LUT of PROSAIL runs (size = 5000) for each remote sensing image based on ~~a given prior . Equations (??, ?? and the prior (Table ??), and the solar and observation angles provided by Sentinel-2 and Lands~~ ~~are~~ then used to evaluate the RL where j is the index of pixels in the simulated image, i ~~is~~ the index of the PROSAIL runs in the ~~LUT and o of , and o is~~ the observed reflectances from the Sentinel-2 or Landsat-8 images. ~~The prior used for the LUT generation is shown~~ PROSAIL provides LAI and not GLAI, the chlorophyll content (cab) is constrained to a high interval [60,80] $\mathrm{ug\,m^{-2}}$. This ~~forces all considered foliar surfaces to be makes all simulated surfaces~~ green and thus allows to ~~inverse retrieve~~ GLAI. A con-

~~straint~~ is also added ~~on~~ ~~to~~ the relation between dry ~~Biomass~~ ~~biomass~~ and GLAI to reduce the parameter search space by elimi-~~nating~~ solutions with leaves that are too thin or thick. Then, the surface reflectances of the ~~Level2-A~~ ~~Level 2-A~~ BOA products ~~considered~~ to follow a normal distribution with ~~mean and a~~ ~~mean and a~~ standard deviation that is ~~considered constant~~ ~~fixed~~ at ~~0.0~~2. Finally~~the a posteriori~~ , ~~the posterior~~ distribution is approximated with a normal distribution, using ~~Eq.(??) and (??)~~ ~~Equation ??~~ to ~~det~~ermine mu and sigma.

~~2.4.2~~ Application of BASALT to SAFYE-CO2

The simulated variables, DAM, yield, GPP, ~~ecosysthem respiration Recoand NEE~~ ~~Reco, and NEE,~~ are highly dependent on the duration and intensity of ~~the~~ crop development (**?**). The GLAI outputs from PROSAIL are assimilated into SAFYE-CO2 to correct the ~~naive~~ prior vegetation dynamics. This is done by generating ~~a~~ an LUT of SAFYE-CO2 runs (size = ~~10000~~5000) for each zone with the same forcing (*i.e.*, same prior). In this case, the zoning is defined by the weather forcing data (*i.e.* SAFRAN at 8 km). For each zone, ~~equations Eq.(??),(??) and (??)~~ ~~Equations ?? and ??~~ are applied to evaluate the RL given the GLAI observations, where j is the index of pixels in the simulated area, i ~~is~~ the index of ~~for~~ the SAFYE-CO2 runs in the LUT, and o the observed GLAI at different dates. The priors for LUT generation for ~~the~~ SAFYE-CO2 are shown in Table **??**. Those priors are used for the SAFYE-CO2 LUT generation and were reassessed in terms of statistical distribution from (**?**) to account for the high-spatial heterogeneity that can be observed at ~~regional scale~~~~a regional scale and the vegetation cycles that are more contrasted at the pixel le~~ For each parameter~~,~~ a truncated normal distribution is ~~sampled with parameters~~ ~~independently sampled considering~~ mu, sigma, min~~and max independently~~~~, and max values~~; the only exception is PRTwhich has an exponential behaviour. For this parameter, a logarithmic transformation is applied ~~on~~ to the distribution. To aggregate the SAFYE-CO2 simulations at the field scale, the ~~likelyhoods are~~ likelihood is summed over all the pixels in the field ~~??. Eq. (??)and Eq. (??) are~~ (Equation **??**). Finally, Equation **??** is used to compute ~~the mean~~ mu and sigma for a parameter or a variable ~~at~~ on a given day for a field or pixel.

3 Application for wheat in ~~South-West~~ Southwest France~~over Wheat~~

~~In the aim of validating and demonstrating the capabilities of AgriCarbon-EO, a 110x110 km region defined by the 31TCJ~~

3.1 Experimental setup and study area description

Several assimilation experiments were conducted to answer the specific objectives of the paper, they are summarized in Table **??**. The experiments correspond to simulations over the Sentinel-2 31TCJ tile located in ~~South-West of France has been chosen. In this zone the chain is applied over a~~ the southwestern of France for winter wheat in ~~years~~ 2017, 2018, and 2019 (Figure 2). ~~Several assimilation experiments were conducted to answer the specific objectives of the paper, they are summarised in Table ??. They alternate~~ They alternate between the use of S2 alone and the combined use of S2 and L8. ~~Pixel and field scales are also considered~~They also include pixel and field scale simulations. The ACEO-S2L8-Pixel combines Landsat-8 and Sentinel-2 data at 10 m resolution which represents ~~about~~ approximately 20 M pixels for our study area. It ~~is~~ was used as the main simulation for the validation experiments. The ACEO-S2L8-Field simulations correspond to averaging the 10 m GLAI from

PROSAIL ~~retrieval at~~ retrievals at the field scale. Additionally, an averaging of the ~~high resolution~~ high-resolution simulations with Sentinel-2 and Landsat-8 ~~is performed at~~ was performed at the field scale (ACEO-S2L8-Mean).

~~Chronogram of the used remote sensing dataset from Sentinel-2A (S2A), Sentinel-2B (S2B) and Landsat-8 (L8), over the 31TCJ tile for years 2016 to 2019. The bars plots represent the percentage of cloud-free pixels for each image.~~

3.2 ~~Study area~~

~~The region of interest is covered by tile 31TCJ (Figure 2). It is also part of the Space Regional Observatory that benefits from extensive validation data that are used in this study and presented in Section 3.2. The region~~ The study area has a mean annual precipitation of 655 mm and a mean annual temperature close to 13 °C. It is classified as a majorly temperate oceanic climate (Cbf) in the ~~plain~~plains, and temperate continental climate (Dfb) near the Pyrénnées mountains, based on the Koppen climate classification. In ~~year~~ 2017, winter was exceptionally dry and sunny, and spring was sunny with a 10 % deficit in rainfall (**?**), while ~~year~~ 2019, had a mild winter and a sunny spring with 10 % deficit rainfall for the two seasons (**?**). The region has an intermediary cloud coverage that allows for ~~multi-temporal~~ multitemporal optical remote sensing analysis and analysis of the impact of clouds (Figure ~~**??**~~2.B). It is mainly occupied by agricultural fields that cover ~~about~~ approximately 90 % of the area, among which a majority of seasonal crops. Winter wheat covers ~~around~~ approximately 20 % of the zone and reaches 40 % in some areas. In South-West France, soft-wheat varieties are predominant, and they are usually sown in autumn around mid to end ~~October. They represent~~ of October. Soft wheat represents 75 % of the French exports of ~~soft-wheat~~soft wheat. The crop typically develops slowly during the winter, and growth accelerates during spring. It is harvested from mid-June to the end of July depending on maturation as well as climatic conditions to ~~optimise grainquality from mid June to end of July~~optimize grain. The harvest in 2017 was ~~in the norm~~ normal (6 $\mathrm{t\,ha^{-1}}$ at 15 % humidity), while 2019 was an ~~exceptionally good~~ exceptional year with a yield of 11.5 $\mathrm{t\,ha^{-1}}$ at 15 % humidity (**?**). In terms of pedology, two main soil ~~classes cover~~ types are present in the area of study: ~~silt rich~~ silt-rich soils near the major streams, and clay soils across the hills with a variable density of stones depending on erosion. The topography offers a wide range of ~~expositions~~aspects. The region also bears the effects of ~~the~~ historical land management, specifically, the "Remembrement" policy, a political push to merge adjacent fields from 1945 to 1980 in France (**?**). This leads to a wide range of soil and ~~micro-climatic~~ microclimatic conditions that cause significant ~~intra-field~~ intrafield plant growth variability.

This study area was chosen for three main reasons in light of the aims of the paper. First, it is part of the Space Regional Observatory that benefits from extensive datasets regarding crop growth and crop physiology through the presence of two certified ICOS flux sites (FR-AUR and FR-LAM), and extensive measurement campaigns operated by different public laboratories specializing in agronomy and remote sensing as well as measurement campaigns operated by private companies and individual farmers. These measured variables related to the field's carbon budget such as NEE, GPP, Reco, DAM, and Yield (Equations **??** and **??**) are monitored in different localities with different representative scales (Table 3.2). Second, the crop growth and biophysical process variability, due to topography and pedo-climatic variations, is needed to assess the impact of using high-resolution modelling and assimilation schemes in quantifying the carbon budget components (e.g. Yield, $CO-2$ fluxes). Third, winter wheat is one of the most studied crops worldwide. This allows us to compare the quality of the results obtained

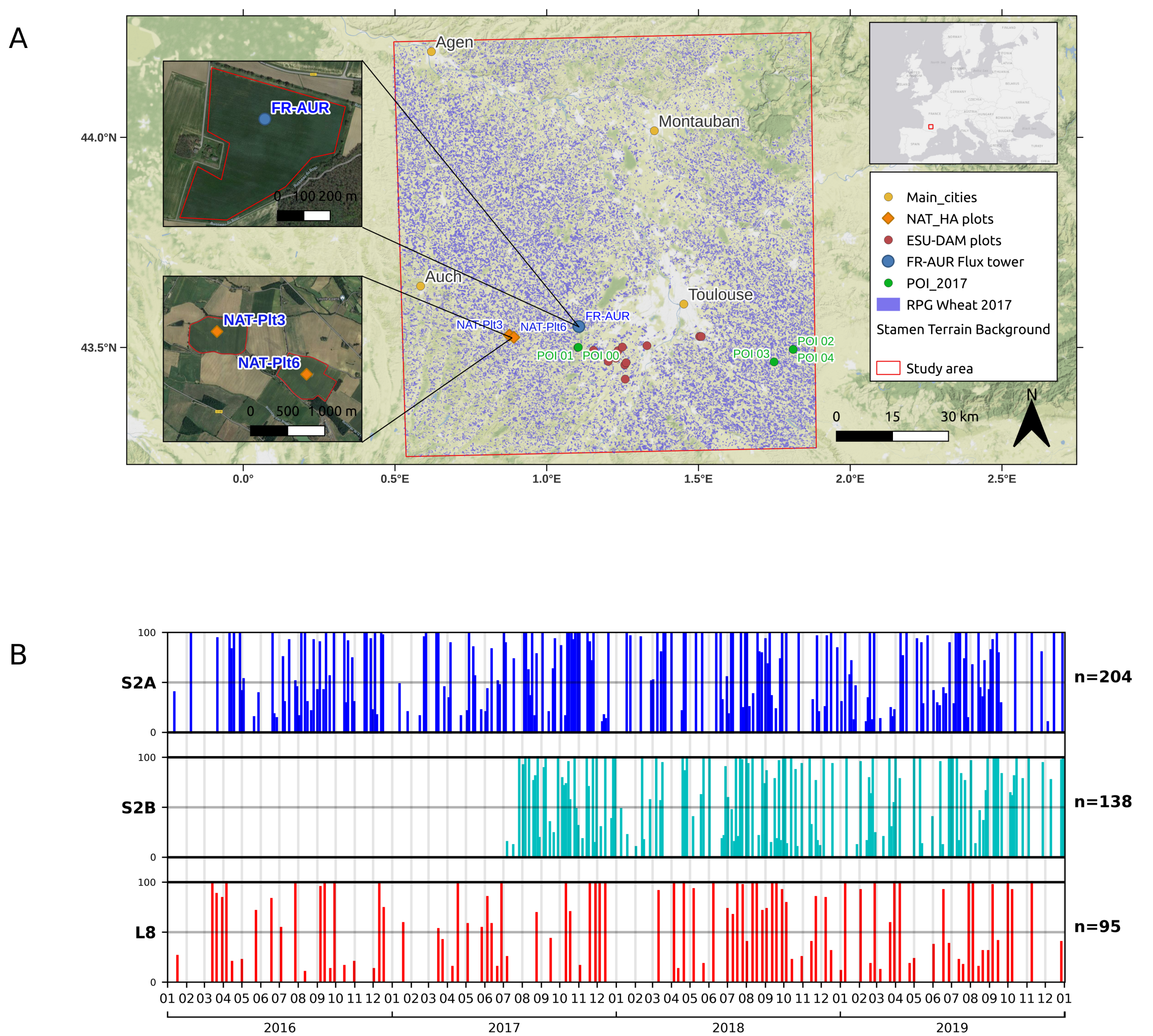

Figure 2. Map of the simulation area and image availability from 2016 to 2019. In "A": ~~in~~ background the ~~terrain map~~ESRI World Topo Map, ~~tile~~ the 31TCJ ~~limts~~ Sentinel2 tile limits (red rectangle), land cover for winter wheat fields for 2017 (blue), location of the FR-AUR ~~flux towers (blue circle)~~ICOS site, the Dry Above ground Biomass (DAM) measurements ~~for ESU-DAM~~ (red circles) ~~,~~ and the two fields monitored with connected combine harvester (CH) (orange circles). ~~Zoom~~ The zoomed maps show the FR-AUR field and the ~~combine harvester~~ fields monitored using combine harvesters. In "B": Chronogram of the remote sensing dataset from Sentinel-2A (S2A), Sentinel-2B (S2B) and Landsat-8 (L8), over the 31TCJ tile for 2016 to 2019. The bar plots represent the percentage of cloud-free pixels for each image.

with AgriCarbon-EO against a large corpus of published studies. Furthermore, the area is a dense crop production zone. This is especially true for wheat production, which has a large economic interest.

3.2 Validation ~~datasets~~of the AgriCarbon-EO outputs

The validation ~~is based~~ relies on several datasets ~~covering~~ corresponding to the main output variables of AgriCarbon-EO: CO-2 flux measurements (*i.e.* ~~Net Ecosystem Exchange, NEE; Gross Primary Production, GPP; Ecosystem Respiration~~NEE, GPP, Reco)~~; Dry Aboveground biomass~~, DAM measurements over Elementary Sampling Units (ESU), and yield maps. A summary of the ID and characteristics of the aforementioned validation datasets is presented in Table **??**. The validation datasets ~~are~~ were extracted from the database of the Environmental Information System ~~the laboratory and the Regional Spatial Observatory (RSO). his Information systhem centralises the in-situ datasets of the RSO including the data from the ICOS flux towers located in the RSO (e.g. FR-AUR) (?). In addition to the validation exercise, the large scale spatial maps from AgriCarbon-EO are analysed with respect to soil texture provided at 250 m resolution from SOILGRIDS and Digital Elevation Model (DEM) provided by the European Environmental Protection Agency (EPA). The validation strategy covers a wide range of spatial and temporal scales. Figure **??** shows the spatial and temporal representativity of the inputs, the validation datasets, the regional datasets, and AgriCarbon-EO outputs. Temporal and spatial coverage of the input dataset (S2,L8, SAFRAN, and RPG), the validation dataset (Eddy covariance, Biomass, and Combine harvest), the regional dataset (SOILGRIDS and DEM), and AgriCarbon-EO outputs (blue zone).~~ maintained by the CESBIO laboratory (**?**).

3.2.1 ~~CO-2 fluxes from eddy covariance~~

~~The CO-2 fluxes components GPP, Reco and NEE are provided from the ICOS site at Auradé France (FR-AUR) using the~~

3.2.1 Validation against field scale CO_2 fluxes and DAM measurements

The FR-AUR ICOS site provides many biophysical measurements, among which variables of interest regarding the carbon budget GPP, Reco and NEE (FR-AUR C-Flux, Table **??**). These variables allow us to assess the soundness of the representation of $CO-2$ fluxes caused by physiological processes in the model, as GPP represents photosynthesis and Reco the sum of plant and soil respiration. Furthermore, NEE allows access to the representation of the biological part of the carbon budget and DAM is linked to carbon export (Equation **??**) and NPP (Equation **??**). As one of the requirements for the ICOS certification is the homogeneity of the ecosystem, the measurements were considered to be representative of the field. The DAM and $CO-2$ flux measurements were acquired using the ICOS destructive biomass sampling protocol (**?**) and eddy covariance (EC) flux tower measurements processed with EdiRe software (**?**)~~and~~, following the CarboEurope-IP recommendations for data filtering, quality control, and gap filling (Table **??**). The ~~computation is based on the Eddy-Covariance (EC) method for CO-2 which consists in measuring at 20 hz~~ EC method consists of measuring the 3D wind fluctuations ~~using a high frequency~~ at 20 hz using a high-frequency sonic anemometer and the ~~CO-2 concentration using an open path~~ $CO-2$ concentration using a gaz analyser. The covariance is then computed between the turbulent component of the vertical wind and the turbulent component of the

~~CO-2~~ CO – 2 concentrations (?). The ~~CO-2 flux data was considered representative of the FR-AUR. The NEE corresponds to the sum of the CO-2 fluxes and the changes in CO-2 storage around the EC devices. The~~ NEE was then partitioned into ~~gross primary production (GPP) and ecosystem respiration (Reco)~~ GPP and Reco using a formulation for croplands ~~(?)~~ in **?** adapted from (?).

3.2.2 ~~Vegetation biomass from destructive samples~~

~~The dry above ground biomass is obtained from ICOS (FR-AUR-DAM) and from Elementary Sampling Units (ESU-DAM) (Table **??**). In the ESU protocol, the above ground vegetation is sampled with five points following a cross pattern inscribed in a 10 x 10 m square; each sample corresponds to a one linear meter of the crop row. The five samples are weighed fresh in the field. In the lab one of the five samples was dried to retrieve the relative humidity, which is then applied to the five fresh weight measurements to obtain dry above ground biomass. The mean and standard deviation are computed to obtain a representative DAM~~ ~~($\mathrm{g\,m^{-2}}$)~~ ~~for the ESU. Eight fields were also sampled using the ESU protocol in 2018.~~

3.2.2 ~~Yield maps from combine harvester~~

~~Yield maps are provided by a farmer for the Gers department. Data from two fields NAT-Plt3 and NAT-Plt6 (Table **??**) were produced by a combined harvester (CH) that measures the incoming flow of grain, its humidity as well as its position at a fixed frequency with a GPS. These measurements are integrated between two points of~~ Depending on wind speed and the ~~trajectory taking into account harvesting width to compute the grain production (yield) per surface area. Grain humidity content enables the computation of the dry yield mass~~ ~~($\mathrm{g\,m^{-2}}$)~~~~. The point yield data is then converted into a harvest map over the simulation grids by summing the points inside each pixel. A Gaussian smoothing filter with sigma = 12 m is then applied over these maps to reduce the aliasing effects. The spatial anomaly (*i.e.* (value-mu)/sigma) maps are also computed.~~

4 ~~Validation against flux towers and fields data~~

intensity of the turbulence, a fraction of the direct measurements are not representative of the plot, and those data points were filtered out during the processing and replaced with simulated values extrapolated from the environmental conditions. We maintained only daily data points where more than 50% of the information comes from real measurements, as gap-filling over long periods induces high errors (?). The days when less than 50% of the information is provided by measurements are represented in grey in Figure **??**. Furthermore, it is also noticeable that the observed Reco in 2018-2019 dips to zero during the vegetation growth period, which is related to an error in the partitioning process of NEE into GPP and Reco. This period is also ignored for GPP and Reco and is represented in red in Figure **??**.

3.1 ~~Validation of carbon fluxes with flux towers data~~

~~GPP 0, Reco 0.93) and NEE, the three main components of the CO 2019 fluxes~~ R^2 0.95) in 2016 – 2017 ~~FR-AUR~~ 2018 2019 (R^2 = ~~flux site.~~ In this exercise, the daily outputs from AgriCarbon-EO at 10 m resolution ~~are~~ were spatially averaged over the area

~~of~~ the FR-AUR field (~~Eq. ?? that is~~ Equation ??) sampled by the EC tower (a.k.a. the target area in the ICOS nomenclature). ~~Figure ?? (a) shows the fitting of predicted GLAI and the assimilated observed GLAI~~Those averaged values were then compared against FR-AUR DAM and FR-AUR C-Flux as shown in Figure ??, and the corresponding fitting statistics are shown in Table ??. The statistics were computed for three specific periods, from the 1st Jan to the 1st May, the 1st May to the 1st Jul, and the 1st Oct to the 1st Oct. These periods correspond to the growing and senescence of the wheat crop and the whole cropping year respectively. The GLAI fitting statistics computed over the growing season show a good fit (

~~Figure ?? illustrates the temporal variations of biomass over the FR-AUR field in 2017 and 2019 cropping years, together with the fieldde~~

~~. Also, the modelled~~

~~3.0.1 Validation against spatialised DAM measurements~~

~~The ESU protocol allows the assessment of variables at decametric scales. Among those variables DAM is especially of interest as it can b~~

ground biomass~~dynamics are consistent with the observed ones apart from an overestimation of the simulation in the beginning of the veg~~

~~Dry above ground biomass (DAM) time series with corresponding observations of destructive DAM for winter wheat crop at the FR-AU~~

Figure ?? shows the scatter plot between the simulated and observed DAM ~~at the FR-AUR site (2017 and 2019 cropping years) and ESU~~

The comparison shows a good fit when considering ~~together~~ all DAM measurements with ~~a $R^2 of 0.90, a RMSE of 250$~~ an $R^2 of 0.94, an RM$

~~The yields simulated with AgriCarbon-EO are compared to the CH yield maps of 2019 over 2 fields. Before presenting the results it is imp~~

~~3.0.2 Comparison with high resolution combine harvester yield maps~~

~~Yield maps are of high interest for the evaluation of high-resolution crop models in the context of carbon and precision farming. They pro~~

flow sensor and ~~of~~ the grain moisture content sensor can experience significant sensor drift within the field~~, 2)~~. ~~Moreover,~~ CH yield data processing requires a range of parameters such as lag time settings and distance travelled via GPS measurements, header position, and cut width, all of which contribute to the uncertainty in the measurements (?). ~~In this study, yield CH data were provided~~

~~(value-mu)/sigma) maps were also computed. To complete the processing, the colocalization error between observations and AgriCarbon-~~

The simulated yield maps ~~are obtained from AgriCarbon-EO simulation ID:~~ were obtained from the ACEO-S2L8-Pixel simulation by multiplying the final DAM by ~~the Harvest Index (HI~~ HI (Equation ??). We ~~analyse~~ analysed the results in terms of ~~reproduction the retrieva~~ the spatial patterns as shown in Figure 5. These maps ~~shows~~ show the comparison between the CH yield data and the AgriCarbon-EO yield estimates at the pixel level in $\mathrm{t\,ha^{-1}}$ as well as the spatial yield anomaly. ~~The simulated and observed yields for the 2019 cropping~~ ~~.~~ Overall the observed yields show a larger variability than the simulations and a clear saturation effect is observed in the simulations for the NAT-plt6 field. The AgriCarbon-EO and ~~the~~ CH anomaly maps show ~~high heterogeneity (-2sigma to +2sigma anomaly) with c~~ spatial patterns. ~~Yet~~ However, the spatial patterns are more pronounced over the NAT-Plt3 field than over NAT-Plt6. ~~An RMSE, bias~~RMSEs and R^2 ~~of 0.66 $\mathrm{t\,ha^{-1}}$, -0.38 $\mathrm{t\,ha^{-1}}$,~~ values of 0.12 and ~~0.71 $\mathrm{t\,ha^{-1}}$, -0.40 $\mathrm{t\,ha^{-1}}$, 0.25~~ 0.29 are observed for NAT-Plt3 and NAT-Plt6, respectively. The performances of the yield simulations vary strongly between the two fields. A relatively low RMSE and bias indicate a quite good mean representation of the plots. However, the correlation coefficient is quite low and indicates

~~no~~t all the spatial variability in yield can be captured using this approach. The ~~Low correlation as well as the difficulties~~ small R^2 can h ~~re~~producing the range of yield observed variations ~~of~~ in yield values may be caused by the simple representation of grain ~~bio~~mass allocation through the use of ~~a~~ an HI which does not take into account potential variations ~~of harvest index~~ in the HI due ~~to~~ nutrient availability or crop cycle duration (**?**).

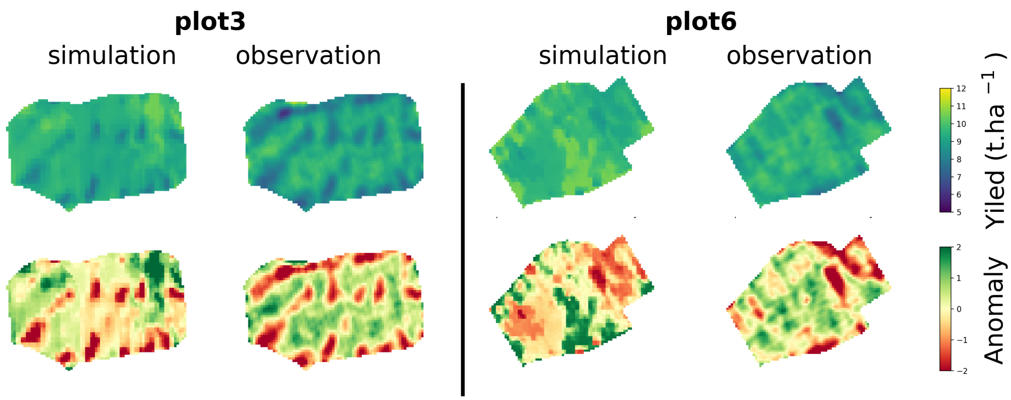

Figure 5. ~~Values~~ Yield maps and spatial ~~anomaly of yield maps~~ anomalies simulated by AgriCarbon-EO and ~~observed yield from~~ collected using a combine harvester over the Nataïs ~~sites~~ site (NAT-Plt3 and NAT-Plt6) for ~~the~~ 2017 and 2019.

~~4 Large scale simulations~~

3.5 ~~Net Ecosystem Exchange, parameter distributions, and singularities~~Large scale simulation outputs

In this section, the results from the ACEO-S2L8-Pixel in 2017 are illustrated and analysed. The RPG ~~shapefile (2017~~ land cover map for wi wheat fields~~)~~, the SAFRAN weather data, and the THEIA S2 and L8 EO data were used as input along with the parametrization files for PROSAIL and SAFYE-CO2. The AgriCarbon-EO processing chain was run in parallel ~~computation~~ over a single server rack with 2 computation nodes and with 36 ~~thread~~ threads max. The memory requirement was the highest for the PROSAIL retrievals ~~reaching 20~~, reaching 5 Gb per process (image inversion) ~~considering 5000 LUT size~~. for a LUT size of 5000. For SAFYE-CO2 the requirements were 5 Gb per process with one process per node of the weather grid ~~considering a 5000 LUT size. A full ch~~ over the 110 x 110 km area of study at 10 m resolution ~~requires~~ required 4 hours of computation time per year of simulation. The chain ~~produces a considerable amount of variables linked to the carbon (and water) cycles at daily scale. Here, we considered the inve La, PRTLb, LUEa, SLA), the DAM at~~ was able to produce maps of all parameters and variables estimated by SAFYE-CO2. With the carb the ~~growing season, the NEP (Net Ecosystem Production)which corresponds to the aggregated NEE over the crop cycle time span (fro~~

The AgriCarbon-EO simulations (Table **??**) were compared at different scales (*i.e.* pixel vs. field) and for different satellite image temporal densities ~~are compared~~ to investigate the benefit of assimilating ~~high resolution multi-mission~~ high-resolution multimission d

GLAI into SAFYE-CO2. The impact of the spatial scale of the GLAI assimilation is illustrated by Figure 8 (a), which shows the histogram of (DAM-ACEO-S2L8-Pixel - DAM-ACEO-S2L8-Field). An average negative bias of -47 $\mathrm{g\,m^{-2}}$ is observed for DAM with a spread between -210 $\mathrm{g\,m^{-2}}$ and +120 $\mathrm{g\,m^{-2}}$ for the [-sigma,+sigma] interval~~,~~ when comparing the pixel scale simulation to the field scale simulation. This result is interpreted as the ~~error in bias induced by considering field scale simulations in the cro~~ be avoided by applying ~~a pixel scale assimilation scheme as in AgriCarbon-EO~~an intrafield assimilation scheme in the crop model in contr Note that the same bias value is obtained for Figure 8 (b) ~~that represents~~ , representing the difference between the averaged pixel at field scale and the field scale simulations: (DAM-ACEO-S2L8-Mean - DAM-ACEO-S2L8-Field). This is mathematically expected as DAM-ACEO-S2L8-Mean is obtained by averaging the DAM-ACEO-S2L8-Pixel simulations. However, when comparing the RMSE values between Figure 8 (a) and (b) a noticeable change in RMSE of -68 $\mathrm{g\,m^{-2}}$ is ~~depicted~~observed. This result shows that the variability of simulated biomass will decrease by 39 % when considering ~~field scale~~ field-scale modelling. The variability is directly influenced by the retrieved parameters of the crop model between the ~~intra-field and field scale~~ intrafield and field the same crop cycle; resulting in a different ~~a posteriori parameter distribution~~posterior parameter distribution, as shown in the section above. Figure 8 (c) shows the difference between a simulation using only S2 and using S2 + L8. Adding L8 images tends to slightly increase dry biomass, with a bias of 30 $\mathrm{g\,m^{-2}}$ and ~~a~~ an RMSE of 94 $\mathrm{g\,m^{-2}}$. This difference is caused by the additional samples added at the start and end of the vegetation cycle that result in a change in the length of the vegetation cycle.

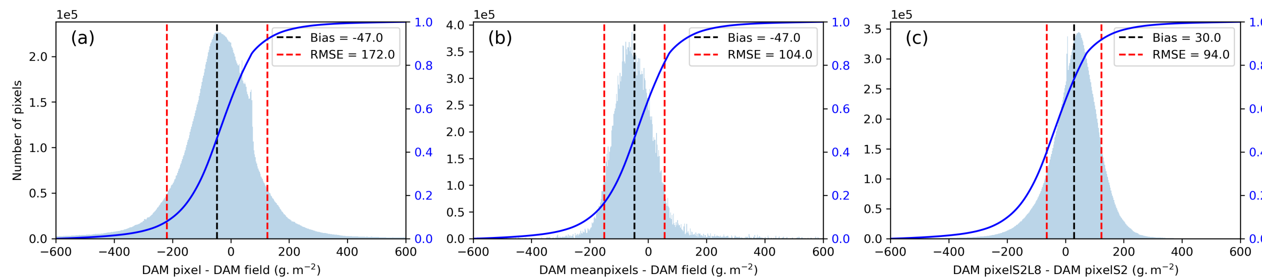

Figure 8. Histogram (left y-axis) and cumulative density function (right y-axis) of the bias of biomass at harvest (y-axis). (a) corresponds to (DAM-ACEO-S2L8-Pixel - DAM-ACEO-S2L8-Field), (b) (DAM-ACEO-S2L8-Mean - DAM-ACEO-S2L8-Field) and (c) (DAM-ACEO-S2L8-Pixel - DAM-ACEO-S2-Pixel).

~~$\mathrm{g\,m^{-2}}$ (for 11 images to 48 $\mathrm{g\,m^{-2}}$ for 28 images) while the DAM of the ... This illustrates the stability of assimilated~~ To extend the results to a broader perspective, the robustness of the assimilation approach ... the variable number of assimilated i ~~the~~ DAM outputs from ACEO-S2L8-Pixel ~~are~~ were analysed in terms of the number of images over each pixel. Figure **??** shows the impact of the number of GLAI observations per pixel on mu and sigma of the DAM. sigma of DAM decreases by ~~about~~ approximately 66 % with the number of observations (146 ~~-~~

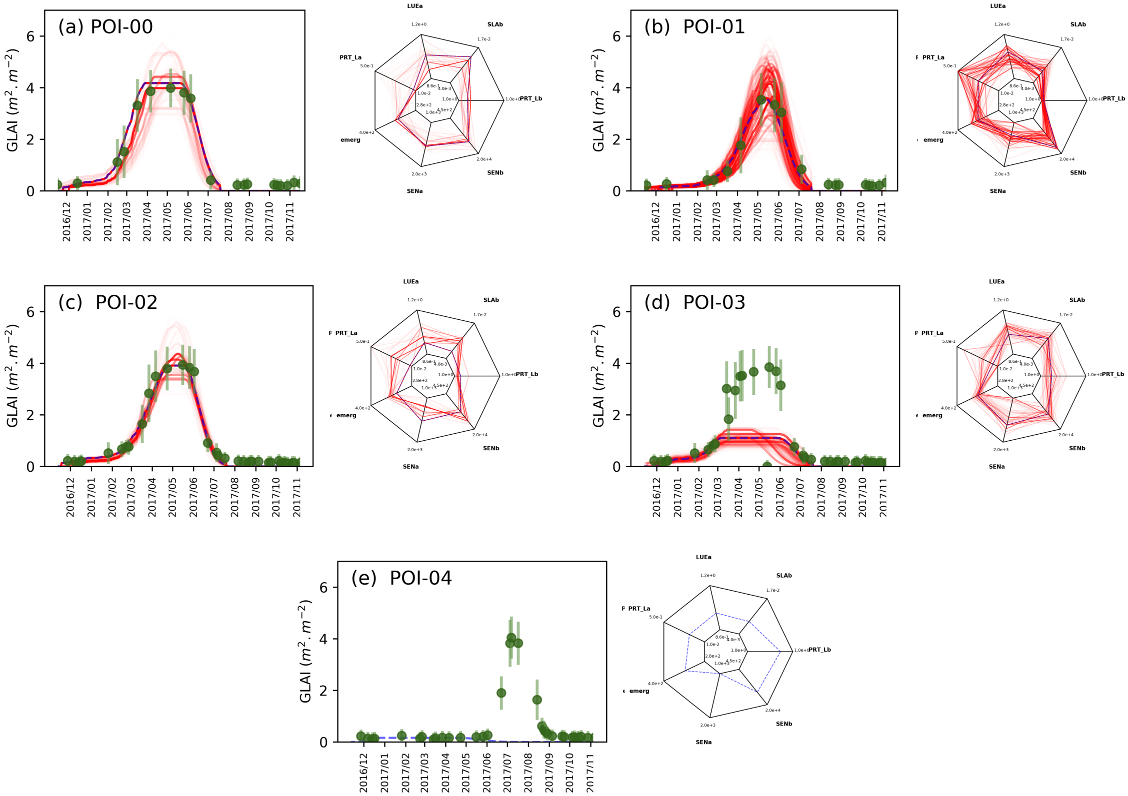

Figure 7. Time series of GLAI, and radar plots containing the free parameters of SAFYE-CO2. Simulations are represented in red with a transparency pr

4 Discussion

~~In this section, the results~~ Quality of ~~AgriCarbon-EO are analysed in relation to potential causes of variability at large and small scales to verify the coherency of the outputs from AgriCarbon-EO based on ACEO-S2L8-Pixel simulation in 2017. Maps of the retrieved parameters and final DAM are generated by applying a Gaussian smoothing with a correlation length of 2.5 km to extract large scale patterns. This scale has been chosen to take into account the values of more than 10 fields which tends to average variety and agricultural practice effects and highlight non field dependent local tendencies. The differences of the raw~~ carbon budget component retrieval]~~Regional scale analysis~~

~~In this section, the results~~ Quality of ~~AgriCarbon-EO are analysed in relation to potential causes of variability at large and small scales to verify the coherency of the outputs from AgriCarbon-EO based on ACEO-S2L8-Pixel simulation in 2017. Maps of the retrieved parameters and final DAM are generated by applying a Gaussian smoothing with a correlation length of 2.5 km to extract large scale patterns. This scale has been chosen to take into account the values of more than 10 fields which~~

~~tends to average variety and agricultural practice effects and highlight non field dependent local tendencies. The differences of the raw~~ carbon budget component retrieval To contextualize the performance of the retrieval of the carbon budget components simulated by AgriCarbon-EO, we compare the results obtained in our study against recent and relevant studies that evaluate at least one of the components that are showcased in this study. Concerning the evaluated variables, the performances are in the range of the scores observed in previous validation exercises with SAFYE-CO2 at the field scale (**?**). When compared to other models, **?** constrained the WOFOST agronomic model with 25 km resolution yield and sowing date data, over 3 ICOS sites comparable to FR-AUR, across Europe. This dataset represents 10 ~~m resolution ans smoothed images gives us the local anomaly. The anomalies highlight the small scale variations that correspond to intra-field and inter-field variability. Figure **??** (b) is produced from the input land cover maps and shows the density of winter wheat fields over the region where the two main winter wheat regions: they correspond to the hilly areas located South-East of Toulouse and to the Gers department (West of Toulouse)~~site-year combinations in total. They obtained R^2 values ranging from 0.64 to 0.74, and RMSE values ranging from 2.33 to 2.67 $\mathrm{g\,m^{-2}}$ for NEE over wheat fields. The values we retrieved for FR-AUR (Table **??**) are higher regarding R^2 and on the low end of values obtained for RMSE, indicating the potential added value of high-resolution agronomic diagnostics. In the ~~valleys, winter wheat is less present as irrigated summer crops (e.g. maize, sunflower) are grown by the farmers. The low winter wheat density around Toulouse agglomeration is also spotted (Figure **??** - a). Figure **??** c to e are obtained~~ same study, GPP was also evaluated and R^2 and RMSE values going from 0.82 to 0.87 and 2.33 to 2.83 $\mathrm{g\,m^{-2}}$were found. The R^2 retrieved from AgriCarbon-EO ~~outputs and they all show large scale spatial patterns. Figure **??** (c) shows that the winter wheat biomass in the far west part of the Gers region was higher than in the other regions which is consistent with the 2017 yield statistics of the ministry of agriculture in France.~~

~~Hydrographic and administrative maps (a) next to Gaussian smoothed maps with 2.5 km correlation length for wheat fields density, biomass (DAM), emergence date (emerg), and start of senescence (sena) (b,c,d,e), respectively.~~

~~To investigate the large scale paterns in the simulations, DAM, emerg and sena are compared to pedological and topographic spatial maps. Figure **??** (a), shows in a ternary plot, the increased DAM and earlier emergence dates with the increased clay content which can be explained by a higher soil water holding capacity. On the other hand, low sena values can be observed for soils with low clay content which is consistent with the fact that early senescence can be caused by a lack of water availability. Finally,~~ is slightly higher, and the ~~emergence date does not seem much affected by the soil texture. Figure **??** (b) shows, in histogram the altitude for positive and negative anomalies of DAM, emerg and sena. A higher number of winter wheat pixels at high altitude tend to emerge earlier than pixels at lower altitudes. This can be seen intuitively given the altitudinal temperature gradient, however this difference may be caused by hill shading effects and hills top effects that allow the higher points to receive more sunlight and wind drying the soils which may promote an earlier warming of the soil and thus germination and emergence. The senescence is also slightly delayed with altitude and the biomass seems to be higher at low altitudes. This later observation can be explained by the fact that in those hilly landscapes, soil depth is smaller at the hills top compared to the bottom of the slope because of soil erosion. It results in low soil fertility and water holding capacities on the hill tops that may reduce biomass production and increase stress which can hasten senescence. Figure **??** (c) shows in radial plots the distribution of expositions (*i.e.* N, W, S, W) given positive and negative anomalies for DAM, emerg and sena considering slopes greater~~

~~than 5%. The radial axis corresponds to the density (*i.e.* a normalised number of pixels). The orange and blue lines correspond to pixels exhibiting positive and negative anomalies respectively. From this figure, it can be observed that the slopes in the region are mainly oriented South-West~~ RMSE was in the same range for 2019 and lower for 2017. The GPP was also analysed using WOFOST at 25 km resolution by assimilating GPP values derived from the MODIS satellite's observations in **?**. In this study, the GPP values were evaluated over 2 years against a flux tower measurement site in Oklahoma (USA). They obtained R^2 values of 0.87 and ~~North-East. Also, the model's output shows that the north eastern exposed fields produce less biomass than the regional mean, while the southern fields show higher biomass. This is consistent with the fact that in the northern hemisphere, northerly exposed slopes receive less incoming solar radiation than the southerly exposed ones, which affects crop photosynthesis and temperature stress. Also differences in the dates of emergence and senescence can be observed between the southerly and northerly exposed areas. The southerly exposed areas tend to emerge earlier and enter in senescence earlier (at a lower degree days values) because of the higher exposition to incoming solar radiation and higher temperatures. Soil on the southern slopes tend to be warmer in the winter which allows an earlier germination and also tend to be drier and hotter during the summer which can also push forward development and senescence. Yet it is also possible that the sum of temperature at senescence is less variable in reality and that the observed variability translates in part to the difference between the real local micro-climate and the 8 km Safran products.~~

~~Impact of texture (ternary plots - a), altitude (histograms - b), and exposition (radial positive and negative anomaly plots - c) on biomass (DAM), emergence date (emerg), and start of senescence (sena). In figures (b) and (c) the orange and blue curves correspond to the ensemble of pixels exhibiting positive and negative anomalies, respectively.~~ 0.67 and RMSE values of 2.26 and 3.25 $\mathrm{g\,m^{-2}}$ in 2015 and 2016, respectively. These values are in the same range as the GPP retrieved by AgriCarbon-EO. The Reco is rarely evaluated by models, as it implies simulating plant and soil processes simultaneously. **?** retrieved Reco with R^2 values ranging from 0.76 to 0.83 and RMSE values ranging from 0.98 to 1.29 $\mathrm{g\,m^{-2}}$. The R^2 obtained with AgriCarbon-EO is slightly lower and the RMSE slightly higher than in (**?**) for Reco. **?**, cited before, also evaluated DAM time series measured at the same flux tower site with RMSE= 121 and 81 $\mathrm{g\,m^{-2}}$ and R^2 =0.94 and 0.93. These statistics concern the whole cropping cycle and can thus be compared against Table **??** for the "all" item and the DAM statistics regarding FR-AUR 2017. AgriCarbon-EO shows a similar variation as in **?**. In **?**, in-situ LAI is assimilated into the LINTUL5 crop model using NIS. The estimations of DAM obtained at maturity (BBCH 99) were compared against field measurements collected on 14 plots located in the Netherlands, northern France, and Germany (from 40 to 60 in-situ sampling points representative of 1 m^2), $showingameanRMSEof246\mathrm{g\,m^{-2}}andameanbiasof58\mathrm{g\,m^{-2}}.Theseresultscanbecomparedtotheend-of-cyclebiomassme$

~~In this section, we discuss the outputs and limitations of our approach from the perspective of the challenges for monitoring the componen~~

4.1 ~~Multi-mission~~ Multimission data, cloud cover, and limitations

The retrieval of SAFYE-CO2 parameters and of the carbon budget components in AgriCarbon-EO relies on the accuracy and availability of EO data~~that~~ , which is hampered by ~~the~~ errors in image ~~co-location, the~~ colocation, atmospheric corrections, the presence of clouds, and ~~the~~ cloud shadow correction. Many studies show that these effects have an important impact

~~in~~ on agricultural remote sensing applications ~~like~~ such as yield estimation (**?**), land cover (**?**~~), or~~ , and superficial soil carbon content mapping (**?**). In our study, we show that these effects are mitigated through the use of a Bayesian approach in a ~~multi-temporal~~ multitemporal context because the uncertainty ~~on the EO derived GLAI are~~ in the EO-derived GLAI is accounted for in the assimilation process. Our approach shows that increasing the number of observations does not strongly impact the mean DAM values, but increases its uncertainty by ~~about~~ approximately 66 %. Nevertheless, unfiltered clouds or the lack of images significantly impact the simulations locally (Figure 7 (c)). ~~The~~ This means that improvements in cloud detection algorithms will highly . The analysis of GLAI time series to detect anomalous variations (Figure 7 (d)) could also be an option to filter clouds. Furthermore, the of additional data from Landsat-8 enhanced the simulation quality for our region of interest. ~~Additional~~ Finally, additional optical or even ~~SAR~~ biophysical variables retrieved from synthetic aperture radar (SAR) satellite data could mitigate the loss of data to cloud cover in northern and coastal regions (**??**). ~~The Improvements in cloud detection algorithms will highly benefit our approach (~~ ~~. The analysis of GLAI time series to detect anomalous variations (Figure 7 (d)) could also be an option to filter clouds.~~

4.2 ~~Importance~~ Impact of ~~high~~ remote sensing and input spatial-resolution

~~Intra-field~~ Intrafield heterogeneity is a ~~well established~~ well-established issue in agricultural applications (**????**~~), but~~ . However, it has not been thoroughly treated in terms of CO-2 fluxes and ~~uncertainties~~ uncertainty estimates. In this paper, we argue that reliable and accurate estimates of DAM and CO-2 fluxes in support of carbon budget ~~components monitoring require intra-field~~ component mo estimates. Our results show that by assimilating ~~mean field~~ mean-field level GLAI products in SAFYE-CO2 a bias of -47 $\mathrm{g\,m^{-2}}$ and an artificial relative uncertainty decrease of 39 % on DAM will be induced compared to assimilating ~~high resolution~~ high-resolution GL and calculating the mean ~~on~~ of the model's output. ~~So high resolution~~ High resolution thus allows more accurate estimates of the mean DAM values at ~~field scale which~~ the field scale, which in turn also enables more accurate ~~field scale~~ field-scale estimates of SOC changes by soil models ~~in the perspective of monitoring SOC stock changes. Still, higher resolutions may need to be investigated t~~ small or elongated fields ~~like for instance in~~ , such as those in rural India (**?**). The other input data products that ~~are driving~~ drive the spatial resolution of the AgriCarbon-EO outputs are the land cover and the weather data. While the land cover is available at an adequate resolution (*i.e.* field sale), it is error-prone, either because of erroneous ~~declarations in the RGP~~ CAP declarations (**?**) or because of classification errors when ~~EO based~~ EO-based land cover maps are used (**?**). Interestingly, our results show that when a mismatch occurs, the fields in question exhibit high anomalies in retrieved parameters and are thus detectable. For the weather forcing, the current application was based on the Météo-France 8 km resolution Safran data, which provides reasonable accuracy over France (**?**). Currently, ECMWF provides ERA5-Land at ~~9 km~~ 0.1° resolution globally (**?**), and NOAA provides ~~HRRR~~ weather reanalysis at 3 km over the US (**?**). In the future, the coverage and resolutions of ~~weather forcing~~ weather-forcing data are expected to increase (*i.e.* ERA6 at 2.5 km). Increasing the resolution of the weather forcing in AgriCarbon-EO would provide better spatial information ~~,~~ but would also increase the computational demand by a factor of $\gamma astheLUTforSAFYE-CO2$ ~~are~~ $isgeneratedovertheweathergrid($~~$Eq.$~~ $Equation$ **??**$)$. ~~$Where$~~ $TLUTistheprocessingtimeforthegenerationofLUTand\theta isth$

4.3 Limitations of the Bayesian and physically based approach

While the components of AgriCarbon-EO have been tailored to the requirements mentioned in the introduction (large scale, high resolution, uncertainty estimates, and biophysical processes), we ~~showed~~ have shown limits for each of them. For instance~~we show that~~ , the BASALT Bayesian approach can be sensitive to an erroneous observation associated with ~~a~~ low uncertainty (Figure 7 d). A trade-off ~~has to~~ must be made between the variability of the generated solutions, and the number of LUT entries to maintain computational efficiency. A solution could be to consider a joint distribution for prior parameters to propose a better ratio of appropriate solutions ~~(Figure??),~~(?). On the one hand, ~~the radiative~~ radiative transfer modelling is constrained by the spectral library database (?), which may not reflect ground conditions ~~like~~ such as the presence of weeds impacting GLAI retrievals. On the other hand, the crop model predictions will depend on fixed and prior parameters of a given crop~~, and the a posteriori parameters distribution. Note that ixed prior parameters need to be chosen through agronomic knowledge and bi~~

Alternatively, we could have reverted to machine learning approaches that have gained ~~in popularity recently~~ popularity for precision agriculture and soil carbon farming ~~application (?). But~~applications (?). However, while they are powerful tools~~to extract the most of~~

take into account ~~changing~~ climatic conditions and management practices ~~. Therefore physically based approaches are still needed(?)~~

~~. In the future, if the confidence in this approach increases, surrogate ML models could be a good option to consider in order to reduce co~~

and need to be updated regularly as we encounter unprecedented weather conditions. Hybrid solutions such as AgriCarbon-EO that combi

In the current state, it is reasonable to consider that an MRV platform for SOC carbon stock changes ~~shall include ensemble approaches (dire~~

varying levels of complexity ~~and involving a diverse array of stakeholders (?)~~ (e.g. Tier 1,2 and 3) (?), similar to what has been implemented in the IPCC approaches (?). In this framework, AgriCarbon-EO is designed ~~with the objective to implement some of these sol~~

4.4 From AgriCarbon-EO to ~~carbon~~ SOC budget

The present approach provides ~~high resolution~~ high-resolution estimates of key carbon budget components ~~using a soil respiration module,~~

SAFYE-CO2 crop model~~, that is decoupled from the soil carbon reservoirs~~currently uses a simplified soil respiration module that simulat

This methodology is adapted for ~~short term ,large scale assessment of the~~ short-term assessment of carbon budgets (typically up to one year) (?). ~~In fact,~~ This means that stock-dependent soil processes that affect ~~soil organic matter mineralisation at longer time scal~~

not accounted for here. The inclusion of a soil carbon decomposition module, as in ?, that ~~describes the different active and stable carbon po~~

soil carbon content~~and organic organic amendments which is challenging for large scale~~ , soil chemical characteristics, and organic amend

One way of achieving this is to take advantage of the rapidly developing Farm's Management Information Systems (FMIS) and enhanced soil ~~properties maps through Digital Soil Mapping~~ property maps through digital soil mapping (DSM). Even though ~~FMIS~~ farmer activity data are not easily accessible, it is expected that this limitation will be reduced with the development of soil carbon farming policies (~~like~~ such as the Label Bas ~~Carbon) and the~~ Carbone in France) and auditing schemes (?). Such data exchange ~~will~~ would have a dual positive effect~~providing~~ , provided that adequate soil sampling protocols are applied. The SOC data ~~will augment the data collection~~ would increase the size of existing datasets available for validation and verification of tools like AgriCarbon-EO, and at the same time, approaches such as AgriCarbon-EO may provide optimal sampling strategies for the estimation of SOC stock changes for carbon auditing.

5 Conclusion~~and outlook~~

~~This paper presents~~ The main aim of the paper is to present the AgriCarbon-EO processing chain that assimilates remote sensing data into the PROSAIL radiative transfer model and the SAFYE-CO2 crop model to estimate ~~some of the~~ key carbon budget components of crop fields at high resolution and regional scale. AgriCarbon-EO was designed to cover essential features to comply with the monitoring component of the MRV systems for cropland carbon budget (**??**):

1. ~~After detailing the processing chain algorithm and formulation, we presented validation and analysis results, in a multi-scale temporal and~~
 The paper details the mathematical concepts and the algorithm behind the AgriCarbon-EO processing chain. The use of a noniterative B
flux tower measurements, we find that the new inversion approach (BASALT) produces reliable estimates of ~~$Co-2$ fluxes ,~~ $CO-2$ fluxes (
GPP~~and Reco and with similar performances compared to~~ , and Reco) and performs similarly to SAFYE-CO2 in previous studies while providing ~~their associated uncertainties~~ uncertainty estimates. Our estimates for ~~dry aboveground biomass DAM were~~ DAM are cl
to the observations while the validation exercise for yield ~~was~~ is less conclusive due to the small range of yield values, the uncertainty of the ~~combine harvester~~ CH's data and processing, and/or the use of a ~~Harvest Index~~ HI to estimate yield that may not ~~allow the account of a~~
drivers of yield. ~~When applying AgriCarbon-EO at large scale, we show its ability to reproduce the high variability of the outputs at local s~~
analysis of the impact of the number of remote sensing acquisitions ~~show~~ shows a reduction in uncertainty of 66 % when full S2 and L8 data ~~is available~~ are available, while the median retrieved NEE and DAM remained the same. ~~Also, we assessed the importance of th~~
find that the assimilation of field scale GLAI products induces a bias on the DAM ~~of~~ from -120 to 210 $\mathrm{g\,m^{-2}}$ and a reduction ~~of the DAM inter-field~~ in the DAM interfield variability of about 39 % compared to pixel scale assimilation. Based on this, we argue that an ~~intra-field~~ intrafield scale quantification of the ~~DAM and of the biomass that returns to the soil is needed for accurate monitor~~
budget components ~~and the SOC stock changes at~~ NECB is preferable as this resolution provides 1) ~~a~~ coherent spatial information with soil samples. 2) the means to provide better sampling strategies ~~forsoil and plants in MRV approaches. In the future, we aim to~~
remote sensing ~~datasets from SARand other variables derived from optical sensing. Such information will reduce the impact of cloud cove~~
AgriCarbon-EO can also provide variables related to the water cycle such as soil moisture, evaporation, transpiration, ~~drainage as well as so~~
a coherent ~~and multi-criteria full crop cycle agronomic diagnosis tool for production~~ agronomic decision support tool for yield, phenology,
carbon, ~~phenology and water use.~~ and water fluxes.

TW and AA proposed the methodology. TW, AA, and LA developed the chain code. TW and AA conducted the simulations and the visua

The contact authors declare that neither they nor their coauthors have any competing interests.

The source of datasets and codes is given hereafter. Datasets:

Code availability:

AgriCarbon-EO is implemented in python3. AgriCarbon-EO requires the PROSAILv5 python package and the SAFYE-CO2 v2.0.5 python implementation. AgriCarbon-EO v1.0.1 is available free of charge for research and evaluation purposes (non-commercial) upon signature of a licence agreement with the Toulouse Technology Transfer (TTT) office of Université Toulouse 3.

For this, the user contacts the TTT at "contact@toulouse-tech-transfer.com" providing contact information, affiliation, and objective of use. Upon validation of the license, the code is provided by the team at CESBIO. SAFYE-CO2 v2.0.5 is provided with AgriCarbon-EO v1.0.1 in this same procedure. Note that for this paper, and in compliance with the journal requirements, an anonymous procedure was put in place to grant access to the reviewers. PROSAIL: python bindings v2.0.3 for PROSAIL5 is hosted at https://github.com/jgomezdans/prosail and archived under https://zenodo.org/record/2574925#.Y-lIVK3MI2w by Dr.José Gómez-Dans.

References

Allen, R. G., Pereira, L. S., Raes, D., and Smith, M.: Crop evapotranspiration - Guidelines for computing crop water requirements - FAO Irrigation and drainage paper 56, Tech. rep., FAO, 1998.

Amthor, J. S.: The McCree–de Wit–Penning de Vries–Thornley Respiration Paradigms: 30 Years Later, Annals of Botany, 86, 1–20, https://doi.org/10.1006/anbo.2000.1175, https://doi.org/10.1006/anbo.2000.1175, 2000.

ARVALIS: ARVALIS : Toute l'info pour gérer son exploitation agricole, https://www.arvalis-infos.fr/index.html, 2019.

Baetens, L., Desjardins, C., and Hagolle, O.: Validation of Copernicus Sentinel-2 Cloud Masks Obtained from MAJA, Sen2Cor, and FMask Processors Using Reference Cloud Masks Generated with a Supervised Active Learning Procedure, Remote Sensing, 11, 433, https://doi.org/10.3390/rs11040433, https://www.mdpi.com/2072-4292/11/4/433, number: 4 Publisher: Multidisciplinary Digital Publishing Institute, 2019.

Baker, A. R. H.: LE REMEMBREMENT RURAL EN FRANCE, Geography, 46, 60–62, https://www.jstor.org/stable/40565215, publisher: Geographical Association, 1961.

Baldocchi, D. D.: Assessing the eddy covariance technique for evaluating carbon dioxide exchange rates of ecosystems: past, present and future, Global Change Biology, 9, 479–492, https://doi.org/10.1046/j.1365-2486.2003.00629.x, http://onlinelibrary.wiley.com/doi/abs/10.1046/j.1365-2486.2003.00629.x, _eprint: https://onlinelibrary.wiley.com/doi/pdf/10.1046/j.1365-2486.2003.00629.x, 2003.

Baret, F., Jacquemoud, S., Guyot, G., and Leprieur, C.: Modeled analysis of the biophysical nature of spectral shifts and comparison with information content of broad bands, Remote Sensing of Environment, 41, 133–142, https://doi.org/10.1016/0034-4257(92)90073-S, https://www.sciencedirect.com/science/article/pii/003442579290073S, 1992.

Battude, M., Al Bitar, A., Brut, A., Tallec, T., Huc, M., Cros, J., Weber, J.-J., Lhuissier, L., Simonneaux, V., and Demarez, V.: Modeling water needs and total irrigation depths of maize crop in the south west of France using high spatial and temporal resolution satellite imagery, Agricultural Water Management, 189, 123–136, https://doi.org/10.1016/j.agwat.2017.04.018, https://www.sciencedirect.com/science/article/pii/S0378377417301609, 2017.

Bellman, R. E.: Adaptive Control Processes: A Guided Tour, in: Adaptive Control Processes, Princeton University Press, https://doi.org/10.1515/9781400874668, https://www.degruyter.com/document/doi/10.1515/9781400874668/html, 2015.

Blackmore, S., Godwin, R. J., and Fountas, S.: The Analysis of Spatial and Temporal Trends in Yield Map Data over Six Years, Biosystems Engineering, 84, 455–466, https://doi.org/10.1016/S1537-5110(03)00038-2, https://www.sciencedirect.com/science/article/pii/S1537511003000382, 2003.

Bolinder, M. A., Crotty, F., Elsen, A., Frac, M., Kismányoky, T., Lipiec, J., Tits, M., Tóth, Z., and Kätterer, T.: The effect of crop residues, cover crops, manures and nitrogen fertilization on soil organic carbon changes in agroecosystems: a synthesis of reviews, Mitigation and Adaptation Strategies for Global Change, 25, 929–952, https://doi.org/10.1007/s11027-020-09916-3, https://doi.org/10.1007/s11027-020-09916-3, 2020.

Béziat, P.: Effets des conditions environnementales et des pratiques culturales sur les flux de carbone et d'eau dans les agrosystèmes, phdthesis, Université Paul Sabatier - Toulouse III, https://tel.archives-ouvertes.fr/tel-00447499, 2009.

Ceschia, E., Béziat, P., Dejoux, J. F., Aubinet, M., Bernhofer, C., Bodson, B., Buchmann, N., Carrara, A., Cellier, P., Di Tommasi, P., Elbers, J. A., Eugster, W., Grünwald, T., Jacobs, C. M. J., Jans, W. W. P., Jones, M., Kutsch, W., Lanigan, G., Magliulo, E., Marloie, O., Moors, E. J., Moureaux, C., Olioso, A., Osborne, B., Sanz, M. J., Saunders, M., Smith, P., Soegaard, H., and Wattenbach, M.: Management effects on net ecosystem carbon and GHG budgets at European crop sites, Agriculture, Ecosystems & Environment, 139, 363–383, https://doi.org/10.1016/j.agee.2010.09.020, https://www.sciencedirect.com/science/article/pii/S0167880910002537, 2010.

Chapin, F. S., Woodwell, G. M., Randerson, J. T., Rastetter, E. B., Lovett, G. M., Baldocchi, D. D., Clark, D. A., Harmon, M. E., Schimel, D. S., Valentini, R., Wirth, C., Aber, J. D., Cole, J. J., Goulden, M. L., Harden, J. W., Heimann, M., Howarth, R. W., Matson, P. A., McGuire, A. D., Melillo, J. M., Mooney, H. A., Neff, J. C., Houghton, R. A., Pace, M. L., Ryan, M. G., Running, S. W., Sala, O. E., Schlesinger, W. H., and Schulze, E.-D.: Reconciling Carbon-cycle Concepts, Terminology, and Methods, Ecosystems, 9, 1041–1050, https://doi.org/10.1007/s10021-005-0105-7, https://doi.org/10.1007/s10021-005-0105-7, 2006.

Choudhury, B. J.: A sensitivity analysis of the radiation use efficiency for gross photosynthesis and net carbon accumulation by wheat, Agricultural and Forest Meteorology, 101, 217–234, https://doi.org/10.1016/S0168-1923(99)00156-2, https://www.sciencedirect.com/science/article/pii/S0168192399001562, 2000.

Clement, R.: EdiRe Software for Micrometeorological Applications, 2008.

Clivot, H., Mouny, J.-C., Duparque, A., Dinh, J.-L., Denoroy, P., Houot, S., Vertès, F., Trochard, R., Bouthier, A., Sagot, S., and Mary, B.: Modeling soil organic carbon evolution in long-term arable experiments with AMG model, Environmental Modelling & Software, 118, 99–113, https://doi.org/10.1016/j.envsoft.2019.04.004, https://www.sciencedirect.com/science/article/pii/S1364815218307643, 2019.

Combe, M., de Wit, A. J. W., Vilà-Guerau de Arellano, J., van der Molen, M. K., Magliulo, V., and Peters, W.: Grain Yield Observations Constrain Cropland CO2 Fluxes Over Europe, Journal of Geophysical Research: Biogeosciences, 122, 3238–3259, https://doi.org/10.1002/2017JG003937, https://onlinelibrary.wiley.com/doi/abs/10.1002/2017JG003937, _eprint: https://onlinelibrary.wiley.com/doi/pdf/10.1002/2017JG003937, 2017.

D. Grisso, R., J. Jasa, P., A. Schroeder, M., and C. Wilcox, J.: YIELD MONITOR ACCURACY: SUCCESSFUL FARMING MAGAZINE CASE STUDY, Applied Engineering in Agriculture, 18, 147, https://doi.org/10.13031/2013.7775, https://elibrary.asabe.org/abstract.asp?aid=7775&t=3, place: St. Joseph, MI Publisher: ASAE, 2002.

Dai, J., Bean, B., Brown, B., Bruening, W., Edwards, J., Flowers, M., Karow, R., Lee, C., Morgan, G., Ottman, M., Ransom, J., and Wiersma, J.: Harvest index and straw yield of five classes of wheat, Biomass and Bioenergy, 85, 223–227, https://doi.org/10.1016/j.biombioe.2015.12.023, https://www.sciencedirect.com/science/article/pii/S0961953415301951, 2016.

de Gruijter, J. J., McBratney, A. B., Minasny, B., Wheeler, I., Malone, B. P., and Stockmann, U.: Farm-scale soil carbon auditing, Geoderma, 265, 120–130, https://doi.org/10.1016/j.geoderma.2015.11.010, https://www.sciencedirect.com/science/article/pii/S0016706115301269, 2016.

De Jong, J.: Een karakterisering van de zonnestraling in Nederland, Technische Hogeschool Eindhoven, Eindhoven, 1980.

Deininger, K., Monchuk, D., Nagarajan, H. K., and Singh, S. K.: Does Land Fragmentation Increase the Cost of Cultivation? Evidence from India, The Journal of Development Studies, 53, 82–98, https://doi.org/10.1080/00220388.2016.1166210, https://doi.org/10.1080/00220388.2016.1166210, publisher: Routledge _eprint: https://doi.org/10.1080/00220388.2016.1166210, 2017.

Delogu, E., Le Dantec, V., Mordelet, P., Ceschia, E., Aubinet, M., Buysse, P., and Pattey, E.: Improved methodology to quantify the temperature sensitivity of the soil heterotrophic respiration in croplands, Geoderma, 296, 18–29, https://doi.org/10.1016/j.geoderma.2017.02.017, https://www.sciencedirect.com/science/article/pii/S0016706117302677, 2017.

Dowell, D. C., Alexander, C. R., James, E. P., Weygandt, S. S., Benjamin, S. G., Manikin, G. S., Blake, B. T., Brown, J. M., Olson, J. B., Hu, M., Smirnova, T. G., Ladwig, T., Kenyon, J. S., Ahmadov, R., Turner, D. D., Duda, J. D., and Alcott, T. I.: The High-Resolution Rapid Refresh (HRRR): An Hourly Updating Convection-Allowing Forecast Model. Part 1: Motivation and System Description, Weather and Forecasting, -1, https://doi.org/10.1175/WAF-D-21-0151.1, https://journals.ametsoc.org/view/journals/wefo/aop/WAF-D-21-0151.1/WAF-D-21-0151.1.xml, publisher: American Meteorological Society Section: Weather and Forecasting, 2022.

Drusch, M., Del Bello, U., Carlier, S., Colin, O., Fernandez, V., Gascon, F., Hoersch, B., Isola, C., Laberinti, P., Martimort, P., Meygret, A., Spoto, F., Sy, O., Marchese, F., and Bargellini, P.: Sentinel-2: ESA's Optical High-Resolution Mission for GMES Operational Services, Remote Sensing of Environment, 120, 25–36, https://doi.org/10.1016/j.rse.2011.11.026, https://www.sciencedirect.com/science/article/pii/S0034425712000636, 2012.

Duchemin, B., Maisongrande, P., Boulet, G., and Benhadj, I.: A simple algorithm for yield estimates: Evaluation for semi-arid irrigated winter wheat monitored with green leaf area index, Environmental Modelling & Software, 23, 876–892, https://doi.org/10.1016/j.envsoft.2007.10.003, https://www.sciencedirect.com/science/article/pii/S1364815207002010, 2008.

Dumont, B., Leemans, V., Mansouri, M., Bodson, B., Destain, J. P., and Destain, M. F.: Parameter identification of the STICS crop model, using an accelerated formal MCMC approach, Environmental Modelling & Software, 52, 121–135, https://doi.org/10.1016/j.envsoft.2013.10.022, https://www.sciencedirect.com/science/article/pii/S136481521300265X, 2014.

Ellili, Y., Walter, C., Michot, D., Pichelin, P., and Lemercier, B.: Mapping soil organic carbon stock change by soil monitoring and digital soil mapping at the landscape scale, Geoderma, 351, 1–8, https://doi.org/10.1016/j.geoderma.2019.03.005, https://www.sciencedirect.com/science/article/pii/S0016706117320633, 2019.

Fieuzal, R., Marais Sicre, C., and Baup, F.: Estimation of Sunflower Yield Using a Simplified Agrometeorological Model Controlled by Optical and SAR Satellite Data, IEEE Journal of Selected Topics in Applied Earth Observations and Remote Sensing, 10, 5412–5422, https://doi.org/10.1109/JSTARS.2017.2737656, conference Name: IEEE Journal of Selected Topics in Applied Earth Observations and Remote Sensing, 2017.

Féret, J. B., Gitelson, A. A., Noble, S. D., and Jacquemoud, S.: PROSPECT-D: Towards modeling leaf optical properties through a complete lifecycle, Remote Sensing of Environment, 193, 204–215, https://doi.org/10.1016/j.rse.2017.03.004, https://www.sciencedirect.com/science/article/pii/S0034425717300962, 2017.

Garrigues, S., Olioso, A., Carrer, D., Decharme, B., Calvet, J.-C., Martin, E., Moulin, S., and Marloie, O.: Impact of climate, vegetation, soil and crop management variables on multi-year ISBA-A-gs simulations of evapotranspiration over a Mediterranean crop site, Geoscientific Model Development, 8, 3033–3053, https://doi.org/10.5194/gmd-8-3033-2015, https://gmd.copernicus.org/articles/8/3033/2015/, publisher: Copernicus GmbH, 2015.

Gervois, S., Ciais, P., de Noblet-Ducoudré, N., Brisson, N., Vuichard, N., and Viovy, N.: Carbon and water balance of European croplands throughout the 20th century, Global Biogeochemical Cycles, 22, https://doi.org/10.1029/2007GB003018, https://onlinelibrary.wiley.com/doi/abs/10.1029/2007GB003018, _eprint: https://onlinelibrary.wiley.com/doi/pdf/10.1029/2007GB003018, 2008.

Gielen, B., Acosta, M., Altimir, N., Buchmann, N., Cescatti, A., Ceschia, E., Fleck, S., Hörtnagl, L., Klumpp, K., Kolari, P., Lohila, A., Loustau, D., Marańon-Jimenez, S., Manise, T., Matteucci, G., Merbold, L., Metzger, C., Moureaux, C., Montagnani, L., Nilsson, M. B., Osborne, B., Papale, D., Pavelka, M., Saunders, M., Simioni, G., Soudani, K., Sonnentag, O., Tallec, T., Tuittila, E.-S., Peichl, M., Pokorny, R., Vincke, C., and Wohlfahrt, G.: Ancillary vegetation measurements at ICOS ecosystem stations, International Agrophysics, 32, 645–664, https://doi.org/10.1515/intag-2017-0048, http://archive.sciendo.com/INTAG/intag.2017.32.issue-4/intag-2017-0048/intag-2017-0048.pdf, 2018.

Gilhespy, S. L., Anthony, S., Cardenas, L., Chadwick, D., del Prado, A., Li, C., Misselbrook, T., Rees, R. M., Salas, W., Sanz-Cobena, A., Smith, P., Tilston, E. L., Topp, C. F. E., Vetter, S., and Yeluripati, J. B.: First 20 years of DNDC (DeNitrification DeComposition): Model evolution, Ecological Modelling, 292, 51–62, https://doi.org/10.1016/j.ecolmodel.2014.09.004, https://www.sciencedirect.com/science/article/pii/S0304380014004190, 2014.

Gregory, P. J., Johnson, S. N., Newton, A. C., and Ingram, J. S. I.: Integrating pests and pathogens into the climate change/food security debate, Journal of Experimental Botany, 60, 2827–2838, https://doi.org/10.1093/jxb/erp080, https://doi.org/10.1093/jxb/erp080, 2009.

Grieve, B. D., Duckett, T., Collison, M., Boyd, L., West, J., Yin, H., Arvin, F., and Pearson, S.: The challenges posed by global broadacre crops in delivering smart agri-robotic solutions: A fundamental rethink is required, Global Food Security, 23, 116–124, https://doi.org/10.1016/j.gfs.2019.04.011, https://www.sciencedirect.com/science/article/pii/S2211912419300100, 2019.

Guenet, B., Moyano, F. E., Peylin, P., Ciais, P., and Janssens, I. A.: Towards a representation of priming on soil carbon decomposition in the global land biosphere model ORCHIDEE (version 1.9.5.2), Geoscientific Model Development, 9, 841–855, https://doi.org/10.5194/gmd-9-841-2016, https://gmd.copernicus.org/articles/9/841/2016/gmd-9-841-2016.html, publisher: Copernicus GmbH, 2016.

Hagolle, O., Colin, J., Coustance, S., Kettig, P., d'Angelo, P., Auer, S., Doxani, G., and Desjardins, C.: Sentinel-2 surface reflectance products generated by CNES and DLR: methods, validation and applications, in: ISPRS Annals of the Photogrammetry, Remote Sensing and Spatial Information Sciences, pp. 9–15, Copernicus Publications, Nice, France, https://doi.org/10.5194/isprs-annals-V-1-2021-9-2021, https://elib.dlr.de/134558/, 2021.

Hao, S., Ryu, D., Western, A., Perry, E., Bogena, H., and Franssen, H. J. H.: Performance of a wheat yield prediction model and factors influencing the performance: A review and meta-analysis, Agricultural Systems, 194, 103 278, https://doi.org/10.1016/j.agsy.2021.103278, https://www.sciencedirect.com/science/article/pii/S0308521X21002316, 2021.

Hararuk, O., Xia, J., and Luo, Y.: Evaluation and improvement of a global land model against soil carbon data using a Bayesian Markov chain Monte Carlo method, Journal of Geophysical Research: Biogeosciences, 119, 403–417, https://doi.org/10.1002/2013JG002535, https://onlinelibrary.wiley.com/doi/abs/10.1002/2013JG002535, _eprint: https://onlinelibrary.wiley.com/doi/pdf/10.1002/2013JG002535, 2014.

Huang, J., Gómez-Dans, J. L., Huang, H., Ma, H., Wu, Q., Lewis, P. E., Liang, S., Chen, Z., Xue, J.-H., Wu, Y., Zhao, F., Wang, J., and Xie, X.: Assimilation of remote sensing into crop growth models: Current status and perspectives, Agricultural and Forest Meteorology, 276-277, 107 609, https://doi.org/10.1016/j.agrformet.2019.06.008, https://linkinghub.elsevier.com/retrieve/pii/S0168192319302175, 2019.

Jacquemoud, S. and Baret, F.: PROSPECT: A model of leaf optical properties spectra, Remote Sensing of Environment, 34, 75–91, https://doi.org/10.1016/0034-4257(90)90100-Z, https://www.sciencedirect.com/science/article/pii/003442579090100Z, 1990.

Jacquemoud, S., Verhoef, W., Baret, F., Bacour, C., Zarco-Tejada, P. J., Asner, G. P., François, C., and Ustin, S. L.: PROSPECT+SAIL models: A review of use for vegetation characterization, Remote Sensing of Environment, 113, S56–S66, https://doi.org/10.1016/j.rse.2008.01.026, https://www.sciencedirect.com/science/article/pii/S0034425709000765, 2009.

Karhu, K., Mattila, T., Bergström, I., and Regina, K.: Biochar addition to agricultural soil increased CH4 uptake and water holding capacity – Results from a short-term pilot field study, Agriculture, Ecosystems & Environment, 140, 309–313, https://doi.org/10.1016/j.agee.2010.12.005, https://www.sciencedirect.com/science/article/pii/S0167880910003208, 2011.

Kumar, S. V., Mocko, D. M., Wang, S., Peters-Lidard, C. D., and Borak, J.: Assimilation of Remotely Sensed Leaf Area Index into the Noah-MP Land Surface Model: Impacts on Water and Carbon Fluxes and States over the Continental United States, Journal of Hydrometeorology, 20, 1359–1377, https://doi.org/10.1175/JHM-D-18-0237.1, https://journals.ametsoc.org/view/journals/hydr/20/7/jhm-d-18-0237_1.xml, publisher: American Meteorological Society Section: Journal of Hydrometeorology, 2019.

Launay, C., Constantin, J., Chlebowski, F., Houot, S., Graux, A.-I., Klumpp, K., Martin, R., Mary, B., Pellerin, S., and Therond, O.: Estimating the carbon storage potential and greenhouse gas emissions of French arable cropland using high-resolution modeling, Global Change Biology, 27, 1645–1661, 2021.

Liu, S., Peng, D., Zhang, B., Chen, Z., Yu, L., Chen, J., Pan, Y., Zheng, S., Hu, J., Lou, Z., Chen, Y., and Yang, S.: The Accuracy of Winter Wheat Identification at Different Growth Stages Using Remote Sensing, Remote Sensing, 14, 893, https://doi.org/10.3390/rs14040893, https://www.mdpi.com/2072-4292/14/4/893, number: 4 Publisher: Multidisciplinary Digital Publishing Institute, 2022.

Lugato, E., Cescatti, A., Jones, A., Ceccherini, G., and Duveiller, G.: Maximising climate mitigation potential by carbon and radiative agricultural land management with cover crops, Environmental Research Letters, 15, 094 075, https://doi.org/10.1088/1748-9326/aba137, https://doi.org/10.1088/1748-9326/aba137, publisher: IOP Publishing, 2020.

Ma, R., Xiao, J., Liang, S., Ma, H., He, T., Guo, D., Liu, X., and Lu, H.: Pixel-level parameter optimization of a terrestrial biosphere model for improving estimation of carbon fluxes with an efficient model–data fusion method and satellite-derived LAI and GPP data, Geoscientific Model Development, 15, 6637–6657, https://doi.org/10.5194/gmd-15-6637-2022, https://gmd.copernicus.org/articles/15/6637/2022/, publisher: Copernicus GmbH, 2022.

Magnin, L.: La politique agricole commune et les données retardataires, Techniques & Culture. Revue semestrielle d'anthropologie des techniques, pp. 130–143, https://doi.org/10.4000/tc.12329, https://journals.openedition.org/tc/12329, iSBN: 9782713227875 Number: 72 Publisher: Les Éditions de l'EHESS, 2019.

Matthews, H. D., Zickfeld, K., Dickau, M., MacIsaac, A. J., Mathesius, S., Nzotungicimpaye, C.-M., and Luers, A.: Temporary nature-based carbon removal can lower peak warming in a well-below 2 °C scenario, Communications Earth & Environment, 3, 1–8, https://doi.org/10.1038/s43247-022-00391-z, https://www.nature.com/articles/s43247-022-00391-z, number: 1 Publisher: Nature Publishing Group, 2022.

Monteith, J. L., Moss, C. J., Cooke, G. W., Pirie, N. W., and Bell, G. D. H.: Climate and the efficiency of crop production in Britain, Philosophical Transactions of the Royal Society of London. B, Biological Sciences, 281, 277–294, https://doi.org/10.1098/rstb.1977.0140, https://royalsocietypublishing.org/doi/abs/10.1098/rstb.1977.0140, publisher: Royal Society, 1977.

Muñoz-Sabater, J., Dutra, E., Agustí-Panareda, A., Albergel, C., Arduini, G., Balsamo, G., Boussetta, S., Choulga, M., Harrigan, S., Hersbach, H., Martens, B., Miralles, D. G., Piles, M., Rodríguez-Fernández, N. J., Zsoter, E., Buontempo, C., and Thépaut, J.-N.: ERA5-Land: a state-of-the-art global reanalysis dataset for land applications, Earth System Science Data, 13, 4349–4383, https://doi.org/10.5194/essd-13-4349-2021, https://essd.copernicus.org/articles/13/4349/2021/, publisher: Copernicus GmbH, 2021.

Météo-France: Bilans climatiques annuels de 2014 à 2018 | Météo-FranceBilans climatiques annuels de 2014, 2015, 2016, 2017, 2018., https://meteofrance.fr/actualite/publications/les-publications-de-meteo-france/bilans-climatiques-annuels-de-2014-2018, 2019.

Météo-France: 2019 : les bilans climatiques | Météo-France 2019 : les bilans climatiques, https://meteofrance.fr/actualite/publications/les-publications-de-meteo-france/2019-les-bilans-climatiques, 2021.

Nevalainen, O., Niemitalo, O., Fer, I., Juntunen, A., Mattila, T., Koskela, O., Kukkamäki, J., Höckerstedt, L., Mäkelä, L., Jarva, P., Heimsch, L., Vekuri, H., Kulmala, L., Stam, A., Kuusela, O., Gerin, S., Viskari, T., Vira, J., Hyväluoma, J., Tuovinen, J.-P., Lohila, A., Laurila, T., Heinonsalo, J., Aalto, T., Kunttu, I., and Liski, J.: Towards agricultural soil carbon monitoring, reporting, and verification through the Field Observatory Network (FiON), Geoscientific Instrumentation, Methods and Data Systems, 11, 93–109, https://doi.org/10.5194/gi-11-93-2022, https://gi.copernicus.org/articles/11/93/2022/, publisher: Copernicus GmbH, 2022.

Nowak, B.: Precision Agriculture: Where do We Stand? A Review of the Adoption of Precision Agriculture Technologies on Field Crops Farms in Developed Countries, Agricultural Research, 10, 515–522, https://doi.org/10.1007/s40003-021-00539-x, https://doi.org/10.1007/s40003-021-00539-x, 2021.

Parker, W. S.: Ensemble modeling, uncertainty and robust predictions, WIREs Climate Change, 4, 213–223, https://doi.org/10.1002/wcc.220, https://onlinelibrary.wiley.com/doi/abs/10.1002/wcc.220, _eprint: https://onlinelibrary.wiley.com/doi/pdf/10.1002/wcc.220, 2013.

Parton, W. J., Hartman, M., Ojima, D., and Schimel, D.: DAYCENT and its land surface submodel: description and testing, Global and planetary Change, 19, 35–48, 1998.

Paustian, K., Larson, E., Kent, J., Marx, E., and Swan, A.: Soil C Sequestration as a Biological Negative Emission Strategy, Frontiers in Climate, 0, https://doi.org/10.3389/fclim.2019.00008, https://www.frontiersin.org/articles/10.3389/fclim.2019.00008/full, publisher: Frontiers, 2019.

Pique, G., Fieuzal, R., Al Bitar, A., Veloso, A., Tallec, T., Brut, A., Ferlicoq, M., Zawilski, B., Dejoux, J.-F., Gibrin, H., and Ceschia, E.: Estimation of daily CO2 fluxes and of the components of the carbon budget for winter wheat by the assimilation of Sentinel 2-like remote sensing data into a crop model, Geoderma, 376, 114 428, https://doi.org/10.1016/j.geoderma.2020.114428, https://linkinghub.elsevier.com/retrieve/pii/S0016706119321998, 2020a.

Pique, G., Fieuzal, R., Debaeke, P., Al Bitar, A., Tallec, T., and Ceschia, E.: Combining High-Resolution Remote Sensing Products with a Crop Model to Estimate Carbon and Water Budget Components: Application to Sunflower, Remote Sensing, 12, 2967, https://doi.org/10.3390/rs12182967, https://www.mdpi.com/2072-4292/12/18/2967, number: 18 Publisher: Multidisciplinary Digital Publishing Institute, 2020b.

Poeplau, C. and Don, A.: Carbon sequestration in agricultural soils via cultivation of cover crops – A meta-analysis, Agriculture, Ecosystems & Environment, 200, 33–41, https://doi.org/10.1016/j.agee.2014.10.024, https://www.sciencedirect.com/science/article/pii/S0167880914004873, 2015.

Porter, C. H., Jones, J. W., Adiku, S., Gijsman, A. J., Gargiulo, O., and Naab, J. B.: Modeling organic carbon and carbon-mediated soil processes in DSSAT v4.5, Operational Research, 10, 247–278, https://doi.org/10.1007/s12351-009-0059-1, https://doi.org/10.1007/s12351-009-0059-1, 2010.

Porter, J. R., Howden, M., and Smith, P.: Considering agriculture in IPCC assessments, Nature Climate Change, 7, 680–683, https://doi.org/10.1038/nclimate3404, https://www.nature.com/articles/nclimate3404, number: 10 Publisher: Nature Publishing Group, 2017.

Pörtner, H. O., Roberts, D. C., Adams, H., Adler, C., Aldunce, P., Ali, E., Begum, R. A., Betts, R., Kerr, R. B., Biesbroek, R., Birkmann, J., Bowen, K., Castellanos, E., Cissé, G., Constable, A., Cramer, W., Dodman, D., Eriksen, S. H., Fischlin, A., Garschagen, M., Glavovic, B., Gilmore, E., Haasnoot, M., Harper, S., Hasegawa, T., Hayward, B., Hirabayashi, Y., Howden, M., Kalaba, K., Kiessling, W., Lasco, R., Lawrence, J., Lemos, M. F., Lempert, R., Ley, D., Lissner, T., Lluch-Cota, S., Loeschke, S., Lucatello, S., Luo, Y., Mackey, B., Maharaj, S., Mendez, C., Mintenbeck, K., Vale, M. M., Morecroft, M. D., Mukherji, A., Mycoo, M., Mustonen, T., Nalau, J., Okem, A., Ometto, J. P., Parmesan, C., Pelling, M., Pinho, P., Poloczanska, E., Racault, M.-F., Reckien, D., Pereira, J., Revi, A., Rose, S., Sanchez-Rodriguez, R., Schipper, E. L. F., Schmidt, D., Schoeman, D., Shaw, R., Singh, C., Solecki, W., Stringer, L., Thomas, A., Totin, E., Trisos, C., Viner, D., Aalst, M. v., Wairiu, M., Warren, R., Yanda, P., and Ibrahim, Z. Z.: Climate change 2022: impacts, adaptation and vulnerability, https://research.wur.nl/en/publications/climate-change-2022-impacts-adaptation-and-vulnerability, publisher: IPCC, 2022.

Reichstein, M., Falge, E., Baldocchi, D., Papale, D., Aubinet, M., Berbigier, P., Bernhofer, C., Buchmann, N., Gilmanov, T., Granier, A., Grünwald, T., Havránková, K., Ilvesniemi, H., Janous, D., Knohl, A., Laurila, T., Lohila, A., Loustau, D., Matteucci, G., Meyers, T., Miglietta, F., Ourcival, J.-M., Pumpanen, J., Rambal, S., Rotenberg, E., Sanz, M., Tenhunen, J., Seufert, G., Vaccari, F., Vesala, T., Yakir, D., and Valentini, R.: On the separation of net ecosystem exchange into assimilation and ecosystem respiration: review and improved algorithm, Global Change Biology, 11, 1424–1439, https://doi.org/10.1111/j.1365-2486.2005.001002.x, http://onlinelibrary.wiley.com/doi/abs/10.1111/j.1365-2486.2005.001002.x, _eprint: https://onlinelibrary.wiley.com/doi/pdf/10.1111/j.1365-2486.2005.001002.x, 2005.

Roderick, M. L., Farquhar, G. D., Berry, S. L., and Noble, I. R.: On the direct effect of clouds and atmospheric particles on the productivity and structure of vegetation, Oecologia, 129, 21–30, https://doi.org/10.1007/s004420100760, https://doi.org/10.1007/s004420100760, 2001.

Roy, D. P., Wulder, M. A., Loveland, T. R., C.e., W., Allen, R. G., Anderson, M. C., Helder, D., Irons, J. R., Johnson, D. M., Kennedy, R., Scambos, T. A., Schaaf, C. B., Schott, J. R., Sheng, Y., Vermote, E. F., Belward, A. S., Bindschadler, R., Cohen, W. B., Gao, F., Hipple, J. D., Hostert, P., Huntington, J., Justice, C. O., Kilic, A., Kovalskyy, V., Lee, Z. P., Lymburner, L., Masek, J. G., McCorkel, J., Shuai, Y., Trezza, R., Vogelmann, J., Wynne, R. H., and Zhu, Z.: Landsat-8: Science and product vision for terrestrial global change research, Remote Sensing of Environment, 145, 154–172, https://doi.org/10.1016/j.rse.2014.02.001, https://www.sciencedirect.com/science/article/pii/S003442571400042X, 2014.

Seidel, S. J., Palosuo, T., Thorburn, P., and Wallach, D.: Towards improved calibration of crop models – Where are we now and where should we go?, European Journal of Agronomy, 94, 25–35, https://doi.org/10.1016/j.eja.2018.01.006, https://www.sciencedirect.com/science/article/pii/S1161030118300066, 2018.

Sharma, A., Jain, A., Gupta, P., and Chowdary, V.: Machine Learning Applications for Precision Agriculture: A Comprehensive Review, IEEE Access, 9, 4843–4873, https://doi.org/10.1109/ACCESS.2020.3048415, conference Name: IEEE Access, 2021.

SIE: SIE - System d'Information Environementale, https://sie.cesbio.omp.eu/variables.php, 2022.

Skakun, S., Wevers, J., Brockmann, C., Doxani, G., Aleksandrov, M., Batič, M., Frantz, D., Gascon, F., Gómez-Chova, L., Hagolle, O., López-Puigdollers, D., Louis, J., Lubej, M., Mateo-García, G., Osman, J., Peressutti, D., Pflug, B., Puc, J., Richter, R., Roger, J.-C., Scaramuzza, P., Vermote, E., Vesel, N., Zupanc, A., and Žust, L.: Cloud Mask Intercomparison eXercise (CMIX): An evaluation of cloud masking algorithms for Landsat 8 and Sentinel-2, Remote Sensing of Environment, 274, 112 990, https://doi.org/10.1016/j.rse.2022.112990, https://www.sciencedirect.com/science/article/pii/S0034425722001043, 2022.

Skea, J., Shukla, P., and Kılkıs, S.: Climate Change 2022: Mitigation of Climate Change, Tech. rep., Cambridge University Press, Cambridge (MA), USA, https://open.metu.edu.tr/handle/11511/97072, 2022.

Smith, P., Lanigan, G., Kutsch, W. L., Buchmann, N., Eugster, W., Aubinet, M., Ceschia, E., Béziat, P., Yeluripati, J. B., Osborne, B., Moors, E. J., Brut, A., Wattenbach, M., Saunders, M., and Jones, M.: Measurements necessary for assessing the net ecosystem carbon budget of croplands, Agriculture, Ecosystems & Environment, 139, 302–315, https://doi.org/10.1016/j.agee.2010.04.004, https://linkinghub.elsevier.com/retrieve/pii/S016788091000112X, 2010.

Smith, P., Soussana, J.-F., Angers, D., Schipper, L., Chenu, C., Rasse, D. P., Batjes, N. H., van Egmond, F., McNeill, S., Kuhnert, M., Arias-Navarro, C., Olesen, J. E., Chirinda, N., Fornara, D., Wollenberg, E., Álvaro Fuentes, J., Sanz-Cobena, A., and Klumpp, K.: How to measure, report and verify soil carbon change to realize the potential of soil carbon sequestration for atmospheric greenhouse gas removal, Global Change Biology, 26, 219–241, https://doi.org/10.1111/gcb.14815, https://onlinelibrary.wiley.com/doi/abs/10.1111/gcb.14815, _eprint: https://onlinelibrary.wiley.com/doi/pdf/10.1111/gcb.14815, 2020.

Song, X.-P., Huang, W., Hansen, M. C., and Potapov, P.: An evaluation of Landsat, Sentinel-2, Sentinel-1 and MODIS data for crop type mapping, Science of Remote Sensing, 3, 100 018, https://doi.org/10.1016/j.srs.2021.100018, https://www.sciencedirect.com/science/article/pii/S2666017221000055, 2021.

Soriano-González, J., Angelats, E., Martínez-Eixarch, M., and Alcaraz, C.: Monitoring rice crop and yield estimation with Sentinel-2 data, Field Crops Research, 281, 108 507, https://doi.org/10.1016/j.fcr.2022.108507, https://www.sciencedirect.com/science/article/pii/S0378429022000788, 2022.

Soussana, J.-F., Lutfalla, S., Ehrhardt, F., Rosenstock, T., Lamanna, C., Havlík, P., Richards, M., Wollenberg, E. L., Chotte, J.-L., Torquebiau, E., Ciais, P., Smith, P., and Lal, R.: Matching policy and science: Rationale for the '4 per 1000 - soils for food security and climate' initiative, Soil and Tillage Research, 188, 3–15, https://doi.org/10.1016/j.still.2017.12.002, https://www.sciencedirect.com/science/article/pii/S0167198717302271, 2019.

Steinbeiss, S., Gleixner, G., and Antonietti, M.: Effect of biochar amendment on soil carbon balance and soil microbial activity, Soil Biology and Biochemistry, 41, 1301–1310, https://doi.org/10.1016/j.soilbio.2009.03.016, https://www.sciencedirect.com/science/article/pii/S0038071709001242, 2009.

Stevens, A., van Wesemael, B., Bartholomeus, H., Rosillon, D., Tychon, B., and Ben-Dor, E.: Laboratory, field and airborne spectroscopy for monitoring organic carbon content in agricultural soils, Geoderma, 144, 395–404, https://doi.org/10.1016/j.geoderma.2007.12.009, https://www.sciencedirect.com/science/article/pii/S001670610700362X, 2008.

Su, Y.-Z., Wang, F., Suo, D.-R., Zhang, Z.-H., and Du, M.-W.: Long-term effect of fertilizer and manure application on soil-carbon sequestration and soil fertility under the wheat–wheat–maize cropping system in northwest China, Nutrient Cycling in Agroecosystems, 75, 285–295, https://doi.org/10.1007/s10705-006-9034-x, https://doi.org/10.1007/s10705-006-9034-x, 2006.

Suits, G. H.: The calculation of the directional reflectance of a vegetative canopy, Remote Sensing of Environment, 2, 117–125, https://doi.org/10.1016/0034-4257(71)90085-X, https://www.sciencedirect.com/science/article/pii/003442577190085X, 1971.

Supit, I., Hoojer, A., and Diepen, C.: System description of the Wofost 6.0 crop simulation model implemented in CGMS. Volume 1: Theory and Algorithms, 1994.

Tewes, A., Hoffmann, H., Krauss, G., Schäfer, F., Kerkhoff, C., and Gaiser, T.: New Approaches for the Assimilation of LAI Measurements into a Crop Model Ensemble to Improve Wheat Biomass Estimations, Agronomy, 10, 446, https://doi.org/10.3390/agronomy10030446, https://www.mdpi.com/2073-4395/10/3/446, number: 3 Publisher: Multidisciplinary Digital Publishing Institute, 2020.

Trepos, R., Champolivier, L., Dejoux, J.-F., Al Bitar, A., Casadebaig, P., and Debaeke, P.: Forecasting Sunflower Grain Yield by Assimilating Leaf Area Index into a Crop Model, Remote Sensing, 12, 3816, https://doi.org/10.3390/rs12223816, https://hal.inrae.fr/hal-03108921, 2020.

Upreti, D., Pignatti, S., Pascucci, S., Tolomio, M., Huang, W., and Casa, R.: Bayesian Calibration of the Aquacrop-OS Model for Durum Wheat by Assimilation of Canopy Cover Retrieved from VENμS Satellite Data, Remote Sensing, 12, 2666, https://doi.org/10.3390/rs12162666, https://www.mdpi.com/2072-4292/12/16/2666, number: 16 Publisher: Multidisciplinary Digital Publishing Institute, 2020.

Vaudour, E., Gomez, C., Loiseau, T., Baghdadi, N., Loubet, B., Arrouays, D., Ali, L., and Lagacherie, P.: The Impact of Acquisition Date on the Prediction Performance of Topsoil Organic Carbon from Sentinel-2 for Croplands, Remote Sensing, 11, 2143, https://doi.org/10.3390/rs11182143, https://www.mdpi.com/2072-4292/11/18/2143, number: 18 Publisher: Multidisciplinary Digital Publishing Institute, 2019.

Veloso, A., Mermoz, S., Bouvet, A., Le Toan, T., Planells, M., Dejoux, J.-F., and Ceschia, E.: Understanding the temporal behavior of crops using Sentinel-1 and Sentinel-2-like data for agricultural applications, Remote Sensing of Environment, 199, 415–426, https://doi.org/10.1016/j.rse.2017.07.015, https://www.sciencedirect.com/science/article/pii/S0034425717303309, 2017.

Veloso, A. G. M.: Modélisation spatialisée de la production, des flux et des bilans de carbone et d'eau des cultures de blé à l'aide de données de télédétection : application au sud-ouest de la France, These de doctorat, Toulouse 3, http://www.theses.fr/2014TOU30092, 2014.

Verhoef, W.: Light scattering by leaf layers with application to canopy reflectance modeling: The SAIL model, Remote Sensing of Environment, 16, 125–141, https://doi.org/10.1016/0034-4257(84)90057-9, https://www.sciencedirect.com/science/article/pii/0034425784900579, 1984.

Verhoef, W., Jia, L., Xiao, Q., and Su, Z.: Unified Optical-Thermal Four-Stream Radiative Transfer Theory for Homogeneous Vegetation Canopies, IEEE Transactions on Geoscience and Remote Sensing, 45, 1808–1822, https://doi.org/10.1109/TGRS.2007.895844, conference Name: IEEE Transactions on Geoscience and Remote Sensing, 2007.

Vidal, J.-P., Martin, E., Franchistéguy, L., Baillon, M., and Soubeyroux, J.-M.: A 50-year high-resolution atmospheric reanalysis over France with the Safran system, International Journal of Climatology, 30, 1627–1644, https://doi.org/10.1002/joc.2003, https://onlinelibrary.wiley.com/doi/abs/10.1002/joc.2003, _eprint: https://onlinelibrary.wiley.com/doi/pdf/10.1002/joc.2003, 2010.

Vrugt, J. A.: Markov chain Monte Carlo simulation using the DREAM software package: Theory, concepts, and MATLAB implementation, Environmental Modelling & Software, 75, 273–316, https://doi.org/10.1016/j.envsoft.2015.08.013, https://www.sciencedirect.com/science/article/pii/S1364815215300396, 2016.

Wall, D. H., Nielsen, U. N., and Six, J.: Soil biodiversity and human health, Nature, 528, 69–76, https://doi.org/10.1038/nature15744, https://www.nature.com/articles/nature15744, number: 7580 Publisher: Nature Publishing Group, 2015.

Wang, J., Lopez-Lozano, R., Weiss, M., Buis, S., Li, W., Liu, S., Baret, F., and Zhang, J.: Crop specific inversion of PROSAIL to retrieve green area index (GAI) from several decametric satellites using a Bayesian framework, Remote Sensing of Environment, 278, 113 085, https://doi.org/10.1016/j.rse.2022.113085, https://www.sciencedirect.com/science/article/pii/S0034425722001997, 2022.

Wattenbach, M., Sus, O., Vuichard, N., Lehuger, S., Gottschalk, P., Li, L., Leip, A., Williams, M., Tomelleri, E., Kutsch, W. L., Buchmann, N., Eugster, W., Dietiker, D., Aubinet, M., Ceschia, E., Béziat, P., Grünwald, T., Hastings, A., Osborne, B., Ciais, P., Cellier, P., and Smith, P.: The carbon balance of European croplands: A cross-site comparison of simulation models, Agriculture, Ecosystems & Environment, 139, 419–453, https://doi.org/10.1016/j.agee.2010.08.004, https://www.sciencedirect.com/science/article/pii/S0167880910002070, 2010.

Weiss, M., Jacob, F., and Duveiller, G.: Remote sensing for agricultural applications: A meta-review, Remote Sensing of Environment, 236, 111 402, https://doi.org/10.1016/j.rse.2019.111402, https://www.sciencedirect.com/science/article/pii/S0034425719304213, 2020.

Woodwell, G. M. and Whittaker, R. H.: Primary Production in Terrestrial Ecosystems, American Zoologist, 8, 19–30, https://doi.org/10.1093/icb/8.1.19, https://academic.oup.com/icb/article-lookup/doi/10.1093/icb/8.1.19, 1968.

Zhang, Q., Xiao, X., Braswell, B., Linder, E., Baret, F., and Moore, B.: Estimating light absorption by chlorophyll, leaf and canopy in a deciduous broadleaf forest using MODIS data and a radiative transfer model, Remote Sensing of Environment, 99, 357–371, https://doi.org/10.1016/j.rse.2005.09.009, https://www.sciencedirect.com/science/article/pii/S0034425705003044, 2005.

Zhuo, W., Huang, J., Xiao, X., Huang, H., Bajgain, R., Wu, X., Gao, X., Wang, J., Li, X., and Wagle, P.: Assimilating remote sensing-based VPM GPP into the WOFOST model for improving regional winter wheat yield estimation, European Journal of Agronomy, 139, 126 556, https://doi.org/10.1016/j.eja.2022.126556, https://www.sciencedirect.com/science/article/pii/S1161030122001046, 2022.